11512–11536 *Nucleic Acids Research, 2021, Vol. 49, No. 20* *Published online 19 October 2021*
https://doi.org/10.1093/nar/gkab930

Nrd1p identifies aberrant and natural exosomal target messages during the nuclear mRNA surveillance in *Saccharomyces cerevisiae*

Pragyan Singh, Anusha Chaudhuri, Mayukh Banerjea, Neeraja Marathe and Biswadip Das*

Department of Life Science and Biotechnology, Jadavpur University, Kolkata - 700032, West Bengal, India

Received August 27, 2021; Editorial Decision September 22, 2021; Accepted October 16, 2021

ABSTRACT

Nuclear degradation of aberrant mRNAs in *Saccharomyces cerevisiae* is accomplished by the nuclear exosome and its cofactors TRAMP/CTEXT. Evidence from this investigation establishes a universal role of the Nrd1p-Nab3p-Sen1p (NNS) complex in the nuclear decay of all categories of aberrant mRNAs. In agreement with this, both *nrd1-1* and *nrd1-2* mutations impaired the decay of all classes of aberrant messages. This phenotype is similar to that displayed by *GAL::RRP41* and *rrp6*-Δ mutant yeast strains. Remarkably, however, *nrd1*Δ^{CID} mutation (lacking the C-terminal domain required for interaction of Nrd1p with RNAPII) only diminished the decay of aberrant messages with defects occurring during the early stage of mRNP biogenesis, without affecting other messages with defects generated later in the process. Co-transcriptional recruitment of Nrd1p on the aberrant mRNAs was vital for their concomitant decay. Strikingly, this recruitment on to mRNAs defective in the early phases of biogenesis is solely dependent upon RNAPII. In contrast, Nrd1p recruitment onto export-defective transcripts with defects occurring in the later stage of biogenesis is independent of RNAPII and dependent on the CF1A component, Pcf11p, which explains the observed characteristic phenotype of *nrd1*Δ^{CID} mutation. Consistently, *pcf11-2* mutation displayed a selective impairment in the degradation of only the export-defective messages.

GRAPHICAL ABSTRACT

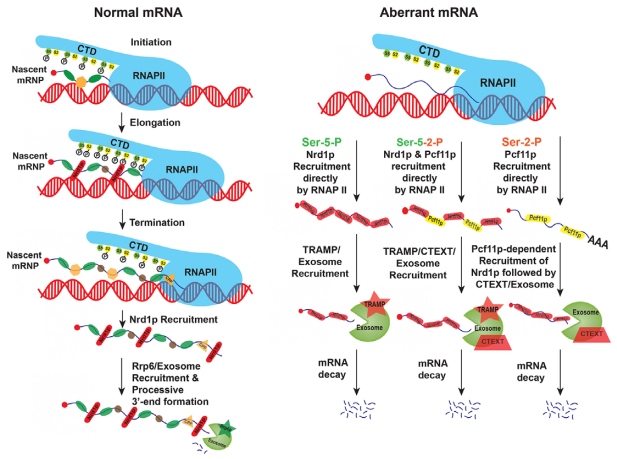

INTRODUCTION

Aberrant messages derived from the inaccurate mRNP biogenesis are eliminated by a broad spectrum of mRNA surveillance and quality control mechanisms (1–4). In *Saccharomyces cerevisiae,* the nuclear exosome and its cofactors degrade a wide array of aberrant and normal mRNAs (1–2,5–8). Functionally, these cofactors recognize specific RNA targets and recruit them further to the core exosome (EXO11$^{Dis3p+Rrp6p}$) to promote their degradation (9). TRAMP (**TR**f4p/5p-**A**ir1p/2p-**M**tr4p-**P**olyadenylation) complex, the best-studied cofactor in *S. cerevisiae* consists of DExH box RNA helicase, Mtr4p (4,10,11), non-canonical poly(A) polymerase, Trf4p/Trf5p and Zn-knuckle RNA binding proteins, Air1p/2p (4,10,11). In addition to TRAMP, two other nuclear cofactors, CTEXT (**C**bc1p-**T**if4631p-dependent **EX**osomal **T**argeting) (previously termed as DRN) (12–16) and NNS (Nrd1p-Nab3p and Sen1p) complexes (17–22), assist the exosome in targeting both aberrant/normal mRNAs as well as a vast majority of ncRNAs (sno-/sn-/CUTS, NUTs and SUTS). CTEXT consists of nuclear

*To whom correspondence should be addressed. Tel: +91 9748908607; Email: biswadipdas22@gmail.com; biswadip.das@jadavpuruniversity.in

cap-binding protein Cbc1p/2p (13,14), shuttling proteins Tif4631p/Upf3p (16), and a DEAD-box RNA helicase, Dbp2p (23), and degrades a distinct group of aberrant (12–16) and normal mRNAs (24–26). The NNS complex, in contrast, comprises Nrd1p and Nab3p as the two major sequence-specific RNA binding proteins (18) and Sen1p as the major DNA-RNA helicase (27) (see below).

Aberrant mRNAs in the yeast nucleus were classified into early, intermediate and late depending on the specific phases of mRNP biogenesis events at which they are generated (Table 1). The transcription-elongation and splice-defective messages were classified as the early, the aberrant 3′-end processing-defective transcripts were categorized as the intermediate, and the export-defective messages were classified as the late category (12). Remarkably, TRAMP and the core exosome are required to degrade faulty messages derived in the early phase of mRNP biogenesis. In contrast, CTEXT and the core exosome complex selectively degrades the export-defective transcripts derived during the late mRNP biogenesis phase (12). Strikingly, the degradation of aberrantly long 3′-extended messages derived at the intermediate stage of mRNP biogenesis requires both the TRAMP and CTEXT along with the nuclear exosome (12). However, the molecular basis of the mRNP-biogenesis stage-specific participation of TRAMP and CTEXT onto the distinct classes of aberrant messages is still unclear.

In *S. cerevisiae*, besides the canonical transcription termination pathway, an alternative transcription termination pathway operates, influencing the stability of a few protein-coding transcripts (21,28). The RNA binding protein Nrd1p (29), complexed with its partners, Nab3p and Sen1p (a putative helicase) (29), dubbed NNS (Nrd1p-Nab3p-Sen1p) complex, plays a pivotal role in transcription termination of pre-snRNAs, pre-snoRNAs, and Cryptic Unstable Transcripts (CUTs) in this alternative mechanism (17–19,22,30–32), thereby leading either to their maturation or degradation by the exosome and TRAMP (20,33). This trimeric complex was demonstrated to bind their RNA targets via the interactions through the elongating RNA Polymerase II (RNAPII) and the nascent RNA (18). Typically, the serine 2 (Ser-2) and 5 (Ser-5) residues of the repetitive C-terminal domain of RNAPII predominantly undergo reversible phosphorylation at various phases of transcription elongation and thereby influence various events of mRNP biogenesis via the recruitment of diverse protein factors involved in these mRNA processing events (34–37). Other than Ser-2 and 5, Tyr-1, Thr-4 and Ser-7 also contribute to the co-transcriptional recruitment of the various processing factors by undergoing reversible phosphorylation (21,38). In the early elongation phase, the Ser-5 and Tyr-1 phosphorylation of the CTD of RNAPII predominates (up to about 100 nucleotides for the yeast genes). After about 100 nucleotides, the phosphorylated ser-5 starts to decrease, and phosphorylated ser-2 starts to increase (38). Although Nrd1 binding is reported to be favored by Ser-5 and Tyr-1 phosphorylation (39,40), the role of Tyr-1 phosphorylation in this process is debatable since several studies have demonstrated that Tyr-1 phosphorylation, which remains very low near the transcription start site (TSS), strongly antagonizes Nrd1p binding (21,38). Nevertheless, binding of Nrd1p and Nab3p to the nascent mRNAs toward the TSS of the protein-coding mRNA (38) subsequently recruits Sen1p helicase, which promotes dissociation of the RNAPII possibly by destabilizing the RNA-DNA hybrid in the transcription bubble (27,39,41,42).

NNS complex directs the decay of antisense mRNA/transcripts and several protein-coding mRNAs (43–47) that include the *NRD1* (to control its expression) (17,19), *URA8, URA2, ADE12* (48,49) and *FKS2* (50) mRNAs. Interestingly, the binding motif to which Nrd1 and its binding partner Nab3p prefer to bind is poorly represented in mRNAs and is highly enriched in sn- and snoRNAs (22). However, Nrd1p and Nab3p were shown to bind to the hundreds of protein-coding mRNAs (22,43–45,51,52), the functional importance of which remained unclear. Although a couple of studies demonstrated a correlation between Nrd1p/Nab3p/Mtr4p binding to stress-responsive messages during glucose starvation with their decay (43,51), the exact nature of the functional role of NNS complex in the decay of these mRNAs remained elusive.

In addition to the normal and functional mRNAs, the NNS complex was also shown to direct the degradation of bacterial Rho factor-induced aberrant transcripts that involved the Nrd1p-dependent coordinated recruitment of Rrp6p after being recruited by the RNAP II (46). Genome-wide high-resolution landscapes of Rrp6p, Trf4p and Nrd1p/Nab3p were utilized to show that Nrd1p/Nab3p appeared to withdraw under normal conditions from mRNA loci and sequester around the sno- and snRNA loci in the genome. Upon activation of the Rho factor that induces the formation of aberrant mRNPs, Nrd1p/Nab3p promptly redistributes from the genomic loci producing non-coding RNAs to the new loci harboring Rho-affected protein-coding genes, thereby triggering their decay and elimination (47). Notably, these researchers did not address if the Nrd1p complex targets all kinds of aberrant messages. Furthermore, the mechanism of action of NNS in the nuclear mRNA surveillance was not explored. In this investigation, we present evidence that Nrd1p (and presumably the NNS complex) plays a central role in the surveillance of all classes of aberrant nuclear mRNAs, and the co-transcriptional recruitment of Nrd1p on all kinds of faulty transcripts is found to be crucial for their decay. Furthermore, Nrd1p-recruitment on the export-defective mRNAs leads to the recruitment of the exosome component Rrp6p. Our evidence suggests that mode of recruitment of Nrd1p onto a given aberrant message is also vital to govern if it would further facilitate the TRAMP- or CTEXT-dependent degradation of a distinct class of faulty messages.

MATERIALS AND METHODS

Nomenclature, strains, media and yeast genetics

Standard genetic nomenclature is used to designate wild-type alleles (e.g. *ACT1*, *CYC1*, *CYH2*, *LYS2*, *HPR1*), recessive mutant alleles (e.g. *lys2-187*, *nup116*-Δ, *nrd1-1, nrd1-2, nrd1*Δ^{CID}) and disruptants or deletions (e.g. *cbc1*::*TRP1*, *cbc1*-Δ, *rrp6*::*TRP1*, *rrp6*-Δ). An example of denoting a protein encoded by a gene is as follows: Nrd1p encoded by *NRD1*. The genotypes of *S. cerevisiae* strains used in this study are listed in Supplementary Table S1. Standard YPD, YPG, SC-Lys (lysine omission) and other omission media

Table 1. Various types of aberrant mRNA substrates, generated progressively during mRNP biogenesis, the specificity of the decay apparatus to degrade them and their representative model mRNAs used in this study.

Stages of mRNP biogenesis	mRNP biogenesis events	Nature of aberrant mRNAs	Specificity of core exosome ($EXO11^{Dis3p+Rrp6p}$)	Specificity of TRAMP	Specificity of CTEXT	yeast mutant strain background used for this study	Representative mRNAs evaluated
Early	Transcription	Transcription assembly defective	+	+	–	*hpr1*-Δ	*ACT1, CYC1*
	Splicing	Intron-containing splice defective	+	+	–	*prp2-1*	pre-*ACT1*, pre-*CYH2*
Intermediate	3′-end Processing	Aberrant transcription termination read-through transcripts with long 3′-Extension	+	+	+	*rna14-1*	*LYS2, CYC1*
Late	Nuclear Export	Export Defective	+	–	+	*lys2-187* mRNA, Nucleus-retained mRNAs in *nup116*-Δ strain, Non-aberrant special mRNAs	*lys2-187* Nucleus retained *ACT1 and CYC1 IMP3, NCW2, SKS1* and *GIC2*

were used for testing and growth of yeast (53). Yeast genetic analysis was carried out by standard procedures (53).

Plasmids and oligonucleotides

The plasmids were either procured from elsewhere or were constructed in this laboratory using standard procedures. All the oligonucleotides were obtained commercially from Integrated DNA Technology (Coralville, IA, U.S.A.). The plasmids and oligonucleotides used in this study are listed in Supplementary Tables S2 and S3, respectively.

Plate assay for suppressibility of the *lys2-187* mutation

A series of 10^{-1} dilution of suspension of 10^5 cells per ml were spotted on YPD, and lysine omission medium (SC-Lys) and the plates were incubated at 30°C for either 3 (for YPD) or 4–5 days (for Sc-Lys) medium followed by capturing the image of the cell growth as described previously (15).

Site-specific mutagenesis

A DNA fragment carrying full-length *NCW2*::*MYC* and *GIC2*::*MYC* marked with a *KAN*MX cassette was transformed into a BY4671 strain background. DNA isolated from this tagged strain was subjected to PCR using different forward and reverse mutagenic primers containing the desired mutations. Amplified PCR products were then transformed into $NRD1^+$, *nrd1-1*, *nrd1-2*, *nrd1*Δ*CID* strains. Transformed cells were subsequently selected on G418 plates. G418 resistant colonies were subjected to DNA sequencing to confirm the presence of the particular mutation. The *ncw2-1, gic2-1* mutant harbors the following mutations respectively T57T (ACU→ACC), V58L (GUA→CUA), and P361P (CCU→CCC), V362L (GUA→CUA).

RNA analyses and determination of steady-state and decay rate of mRNAs

Total RNA was isolated as described earlier (16) by harvesting appropriate yeast strains followed by extracting the cell suspension in the presence of phenol-chloroform-IAA (25:24:1) and glass bead. Following the extraction, the RNA was recovered by precipitation with RNAase-free ethanol. cDNA preparation was initiated by treating the total RNA with DNase I at 37°C for 30 min (Fermentas Inc., Pittsburgh, PA, U.S.A.) to remove genomic DNA. The reaction was stopped by adding 1μl of EDTA and incubating at 65°C for 10 min, followed by first-strand cDNA synthesis using Superscript Reverse Transcriptase (Invitrogen Corporation, Waltham, MA, U.S.A.) using Random Primer (Bioline Inc., Memphis, TN, U.S.A.) by incubating the reaction mixture at 50°C for 30 min. Real-time qPCR analyses were performed with 2–3 ng of cDNA samples for *ACT1*, *CYC1*, *LYS2*, *NCW2*, *SKS1,* etc., and 30 ng for intron-containing splice defective messages, *ACT1* and *CYH2* in *prp2-1* strains to determine the steady-state levels as described previously (16). The decay rate of a specific mRNA was determined by the inhibition of global transcription with transcription inhibitor 1,10-phenanthroline (Sigma-Aldrich India) at 25 or 37°C (as mentioned) and is described previously (16). Briefly, the specific strain was grown at 25°C till the mid-logarithmic phase (special messages), or an additional step was added for temperature-sensitive mutant strains (*hpr1*-Δ, *prp2-1*, *rna14-1*) of shifting the culture from 25 to 37°C for 2 h. This was followed by the addition of 1, 10-phenanthroline to the growing culture at a final concentration of 100 μg/ml and withdrawal of 25 ml of aliquots of culture at various times after transcription shut off. Messenger RNA levels were quantified from cDNA by real-time PCR analysis, and the signals associated with the specific messages were normalized against *SCR1* signals. The decay rates and half-lives of specific mRNAs were estimated with the regression analysis program (Graphpad Prism version

7.04) using a single exponential decay formula (assuming mRNA decay follows first-order kinetics), $y = 100e^{-bx}$ was used.

Real-time PCR

Following the synthesis from total RNA samples, each cDNA was first quantified using Qubit®ds DNA HS Assay Kit (Invitrogen, Waltham, MA, U.S.A.) following the manufacturer's recommendation. Briefly, 2–3 ng of quantified cDNA was used to quantify the levels of specific mRNAs such as *CYC1*, *ACT1*, *IMP3*, *NCW2* and *LYS2* by qPCR assays by using target-specific primers and standard SYBR Green Technology using Power SYBR® Green PCR Master Mix (Applied Biosystems, Waltham, MA, U.S.A.). qPCR assays were run in triplicate and conducted using an Applied Biosystems StepOne™ real-time PCR system followed by the target quantification by the relative quantification (by the $\Delta\Delta^{-Ct}$ method) of individual target mRNAs normalized with respect to *SCR1* RNA. Note that the abundance/steady-state levels of *SCR1* did not change across our experimental condition and various yeast strains (Supplementary Figure S6).

End-point semi-quantitative PCR reaction

PCR was carried with 2–3 ng of quantified cDNA samples using primer sets specific to either *CYC1*, *ACT1*, *IMP3*, *NCW2* and *LYS2* or 50 ng cDNA for splice-defective targets *ACT1* and *CYH2* gene by Taq DNA polymerase (Thermo Fisher Scientific Inc., Waltham, MA, U.S.A.). The conditions for individual PCR reactions varied slightly for individual messages. The PCR products were analyzed on 1% agarose gel, and the signal intensities associated with each band were quantified by ImageJ software (NIH, Bethesda, MD, U.S.A.) from three independent biological replicates.

Protein analyses by western blot

Total protein was isolated from specific yeast strains (WT and *nrd1*Δ^{CID}) grown overnight at 30°C in YPD broth. Following centrifugation at 5000 rpm for 7 min, the cell pellets were quickly frozen in liquid nitrogen and stored at –70°C. Frozen pellets were thawed on ice and resuspended in 1 ml of Buffer A (50 mM Tris–HCl pH 7.5, 150 mM NaCl, 5 mM EDTA, 1 mM DTT, 1 mM PMSF) supplemented with Protease Inhibitor Cocktail (Abcam ab201111, U.K.). The cells were lysed by vortexing 10–15 times with glass beads followed by clarification of the particulate fraction by centrifugation at 11,000 rpm for 20 minutes. Supernatants were collected and saved as the total soluble protein fraction for further analysis. Protein concentration was determined by the Bradford reagent assay kit (Bio-Rad Inc., Valencia, CA, U.S.A.). For Western Analysis, 60 μg of total protein was resolved in 10% SDS polyacrylamide gel. The separated proteins were transferred to the PVDF membrane at 50–100 mA O/N for immunoblotting. Blots were blocked with 5% skimmed milk in Tris-buffered saline (10 mM Tris, 150 mM NaCl, 0.1% Tween 20) and incubated with primary antibodies for specific proteins for 1 h at room temperature in following dilutions in 5% BSA: (i) Rabbit Polyclonal anti-Nrd1 (1:1000) and (ii) Mouse Monoclonal anti-Tubulin (1:2000). Blots were further washed in 1× TBS with 0.1% Tween 20 (TBST) and incubated in HRP-conjugated secondary anti-rabbit or anti-mouse antibody each diluted at 1:3000 in wash buffer for one hour at room temperature. Immunoreactive bands were developed and detected by chemiluminescence (ECL imager kit, Abcam, U.K.), and the images were either captured by X-ray film or by myECL Chemidoc Imager (Thermo Scientific, Waltham, MA, U.S.A.).

Chromatin immunoprecipitation (ChIP) assay

Chromatin preparation was essentially performed following the procedure described earlier (54). The *NRD1*$^+$ and *nrd1*Δ^{CID} strains or *PCF11*$^+$ and *pcf11-2* strains in the different backgrounds were used for this study. Two-hundred fifty milliliters of cells were grown till $OD_{600} \approx 0.5$ ($\approx 10^7$ cells/ml) and were fixed with 1% formaldehyde for 20 min. The reaction was stopped by adding glycine, and the cells were washed and lysed with glass beads to isolate chromatin. The cross-linked chromatin was sheared by sonication to reduce the average fragment size to ≈ 500 bp. Chromatin-IP was carried using the ChIP assay kit (EZ-ChIP™; Cat#17–295) from Merck Millipore, India. Immunoprecipitation of 120 μg Chromatin fractions (≈ 100 μl) from each strain was performed using anti-Nrd1p antibody incubated overnight at 4°C. Incubation with Protein G agarose bead was followed by washing and chromatin elution. The eluted supernatants and the input controls were incubated with Proteinase K for 1 h at 37°C followed by 5 h at 65°C to reverse cross-link the precipitated DNA from the complexes. DNA was purified using the DNA-clean-up column provided with the kit. The immunoprecipitated DNAs (output) were quantified by real-time PCR (as mentioned above) using three sets of primers located along a specific genes coding sequence (5′-end, middle, and 3′-end) and normalized to a half dilution of input DNA. Amplifications were done in duplicate for each sample (technical replicate), averages and standard deviations were calculated based on three independent experiments (biological replicate).

Mining and analysis of the previously deposited PAR-CLIP data

The processed wig files for the Nrd1 Arc Lamp Crosslinking dataset were downloaded from Gene Expression Omnibus (55) found under series number GSE31764 (Originally deposited by Creamer *et al*. 2011) (56). The files were loaded into Integrative Genomics Viewer (57) using which, the Nrd1 PAR-CLIP binding plots were obtained. To find the sites of T → C transition, the raw reads were downloaded from SRA (58) and aligned to the *Saccharomyces cerevisiae* reference genome version R64-1-1, downloaded from https://asia.ensembl.org/ using RNA STAR (59), on the European public server of the galaxy project (https://usegalaxy.eu/) (60). The aligned reads were then investi-

gated for T → C transitions using Integrative Genomics Viewer (57).

RESULTS

We begin this investigation by interrogating if the NNS complex plays a universal functional role to promote the degradation of every class of aberrant nuclear transcripts and further unraveling the functional relationship of NNS with the nuclear exosome/TRAMP/CTEXT. Consequently, we analyzed if mutations in NNS components affect the nuclear decay of the arbitrarily selected representative mRNAs from every class of aberrant messages (Table 1). The analysis was carried out by comparing the steady-state levels and stability of these representative mRNAs from different aberrant classes in isogenic series of yeast strains (Experimental strategy presented in Figure 1A). These isogenic series consist of (i) a parent strain defective in a given type of mRNP biogenesis and (ii) its isogenic derivatives, which additionally harbor various mutations in the *NRD1* gene (Supplementary Table S1 and Figure 1A). The stability analysis was then followed by the systematic investigations of co-transcriptional recruitment profiles of Nrd1p and Rrp6p onto representative model aberrant messages. The recruitment profiles will help us gain insight into how the Nrd1p is recruited to specific types of aberrant messages and what further impact this recruitment has on the downstream fate of these faulty transcripts.

Nrd1p participates in the degradation of transcription elongation-defective mRNAs produced in the THO mutant *hpr1*-Δ yeast strain

During transcription elongation of the protein-coding genes in eukaryotes, a complex of Hpr1p, Tho2p, Mft1p, Thp2 (dubbed THO complex) is deposited on to transcribing messages, which leads to its subsequent association with the splicing/export factors Sub2p/Yra1p to promote their mRNP maturation and export (61–63). Mutation in any THO components (a *hpr1*-Δ or *mft1*-Δ strain) led to the destabilization of several transcripts (61,63,64). Destabilization of these messages was rescued by the inactivation of the nuclear exosome component Rrp6p (*rrp6*-Δ mutation), and TRAMP component Trf4p (*trf4*-Δ mutation) and Mtr4p (*mtr4-1* mutation), but not by the inactivation of CTEXT component Cbc1p (*cbc1*-Δ mutation) (12). The possible role of Nrd1p (and possibly of NNS) in the decay of the transcription assembly-defective mRNAs was evaluated by determining the steady-state levels of Transcription Assembly-Defective (-Tad) forms of two arbitrarily chosen *ACT1* and *CYC1* mRNAs in THO complex-deficient *hpr1*-Δ yeast isogenic strain series at a non-permissive temperature of 37°C either by qRT-PCR or by end-point PCR using gene-specific primer sets (Primer information provided in Supplementary Table S4) (12). As mentioned above, this isogenic series consists of a wild-type parent strain ($HPR1^+$) relative to the strain defective in transcription elongation (*hpr1*-Δ) and derivatives of this defective strain with various mutations in the *NRD1* gene as indicated in Supplementary Table S1. We used three different mutations in the *NRD1* gene (Figure 1B), the first two, *nrd1-1* and *nrd1*-2, harbor pre-mature non-sense mutations leading to the formation of two truncated versions of Nrd1p. The last one, $nrd1\Delta^{CID}$, carries a deletion in its CID (RNAPII **C**TD **I**nteracting **D**omain) that abolishes its ability to interact with RNAPII (20,33) (Figure 1B).

The relative steady-state levels of two representative *ACT1-Tad* and *CYC1-Tad* RNA species determined by qRT-PCR are presented in Figure 1D–E, and G-H as the histograms on the top of each panel, whereas the gel panels at the bottom depict their relative levels as evaluated by end-point PCR (Figure 1D–E and G-H). Remarkably, both the representative *ACT1-Tad,* and *CYC1-Tad* mRNAs displayed a robust stabilization of approximately 7- to 9- (13- to 18-) fold in *hpr1*-Δ *nrd1-1*, *hpr1*-Δ *nrd1-2* and *hpr1*-Δ $nrd1\Delta^{CID}$ strains at the non-permissive temperature of 37°C estimated by qRT-PCR (histograms in Figure 1E and H). Consistently, the pattern of the steady-state levels of these assembly-defective RNAs determined by end-point PCR indeed supports this finding (gel panels in Figure 1E and H). As noted before (12), both *ACT1-Tad* and *CYC1-Tad* transcripts displayed a similar stabilization when exosome component Rrp6p was deleted, but they did not exhibit any stabilization at 37°C when CTEXT component Cbc1p was deleted (Figure 1E and H). Furthermore, no significant alteration in the steady-state levels of these faulty messages was observed in any of these isogenic yeast strain series at a permissive temperature of 25°C (Figure 1D and G). Together, these observations are consistent with the idea that the steady-state levels of these RNAs displayed a dramatic enhancement caused by their diminished decay in *hpr1*-Δ *nrd1* mutant strains. The collective findings support the conclusion that Nrd1p facilitates the rapid degradation of the transcription assembly-defective forms of these mRNAs generated in THO-deficient *hpr1*-Δ strain at the non-permissive temperature of 37°C.

Nrd1p facilitates the degradation of intron-containing pre-mRNAs produced in the splice defective *prp2-1* yeast strain at the non-permissive temperature of 37°C

A mutation in the *PRP2* gene (*prp2-1* allele) encoding an essential splicing factor (65) results in the accumulation of splice-defective pre-mRNAs in the nucleus at a non-permissive temperature of 37°C, which were rapidly degraded by the nuclear exosome (66) and TRAMP complex (12,67) but not by CTEXT complex (12). We evaluated the role of Nrd1p in the decay of the intron-containing pre-mRNAs generated in the *prp2-1* strain at the non-permissive temperature of 37°C by determining the steady-state levels of two randomly selected intron-containing pre-*ACT1* and pre-*CYH2* mRNAs produced in wild-type ($PRP2^+$), *prp2-1* strain and their *nrd1* isogenic derivative series at permissive and non-permissive temperature by qRT-PCR (12). To selectively and precisely detect the precursor forms of these mRNAs, we used a primer set that preferentially amplifies the intron-containing precursor forms and not their mature forms (amplicon location shown in blue line in Figure 2A and C, Supplementary Table S4). Indeed, both the representative pre-*ACT1* and pre-*CYH2* precur-

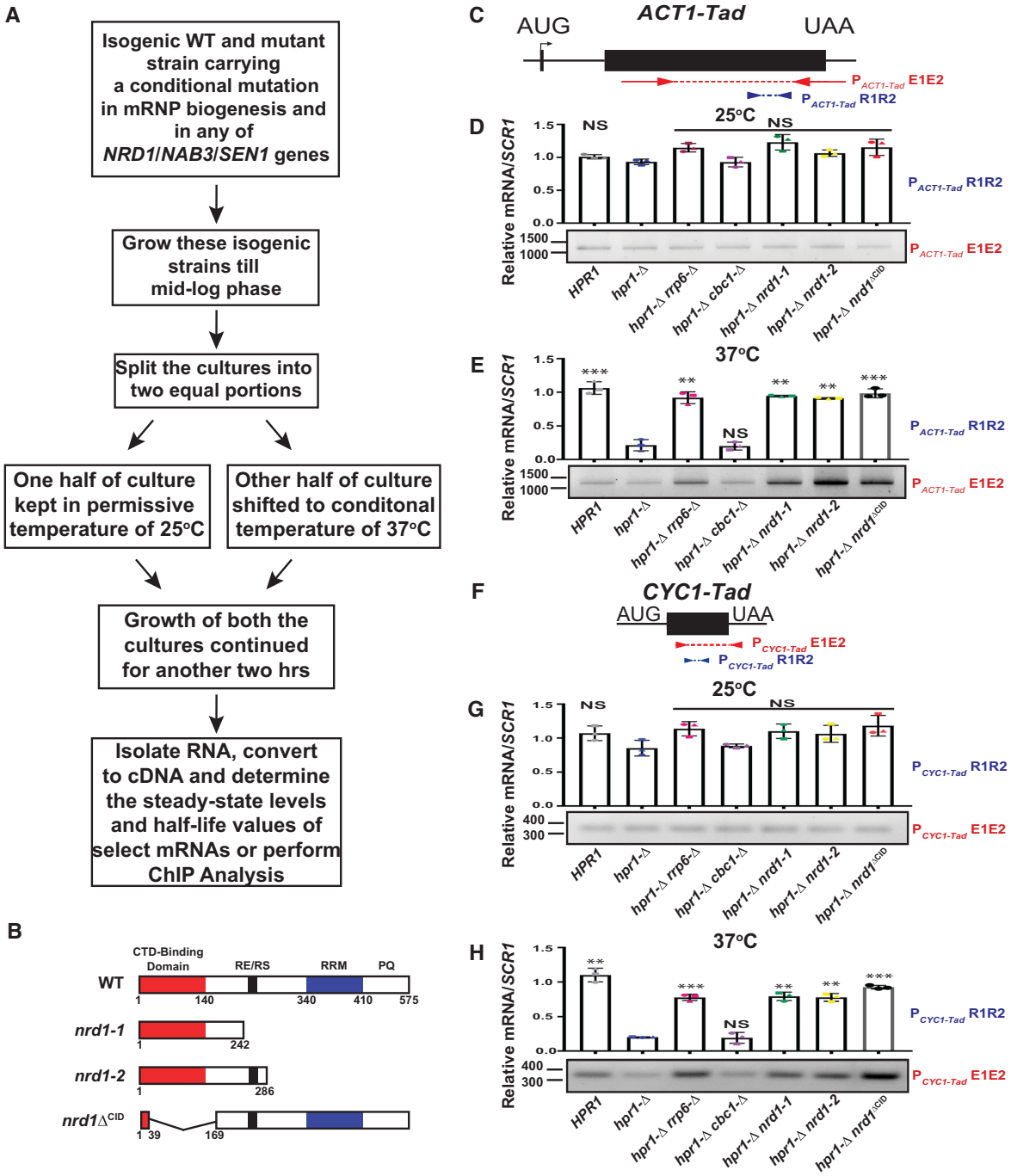

Figure 1. Nrd1p participates in the degradation of aberrant mRNPs generated in transcription-elongation-defective *hpr1*-Δ yeast strain. (**A**) Outline of the experimental procedure used in this investigation. (**B**) Schematic diagram showing the domain organization of full-length Nrd1p (redrawn from reference number (29)): the RNAPII CTD binding domain (CID, aa 1–140), RNA Recognition Motif (RRM, aa 340–410), RE/RS (arginine-, serine- and glutamate-rich region, aa 245–265); and P/Q (proline-, glutamine-rich region, aa 500–575) regions. The specific structures for the *nrd1* mutants are shown below. (**C**–**H**) Relative abundance of transcription assembly-defective (Tad) version of *ACT1*, *ACT1-Tad* (panels C-E) and *CYC1*, *CYC1-Tad* (panels F-H) mRNAs at permissive (25°C) and non-permissive temperature (37°C) in the *HPR1*$^+$, *hpr1*-Δ, and its various isogenic derivative strains as determined by qRT-PCR using either a primer set $P_{ACT1\text{-}Tad}$R1R2 or $P_{CYC1\text{-}Tad}$R1R2 indicated in blue on top and at the right side of the histogram. The mean normalized levels of each target mRNA estimated in the *HPR1*$^+$ sample were set to 1. *P*-value was estimated with respect to the steady-state levels of the transcript in the *hpr1*-Δ yeast strain. The gel panels below each graph depict a representative gel showing the relative levels of the nearly full-length messages as determined by the end-point PCR carried out using either primer set $P_{ACT1\text{-}Tad}$E1E2 or $P_{CYC1\text{-}Tad}$E1E2 (indicated in red on top and at the right side of the gel). Positions of the relevant size standards are shown on the left side of each gel panel. Three independent samples of random-primed cDNA (from biological replicates, $N = 3$) were prepared from indicated strains, pre-grown at 25°C followed by a 2-h shift at 37°C before being subjected to either qRT-PCR or end-point PCR analysis. Transcript copy numbers/3 ng cDNA were normalized to *SCR1* RNA signals obtained from respective samples and are shown as means ± SE. *P* values were estimated from the Student's two-tailed *t*-test for a given pair of test strains for each message and are presented with the following symbols, $*P < 0.05$, $**P < 0.005$ and $***P < 0.001$, NS, not significant.

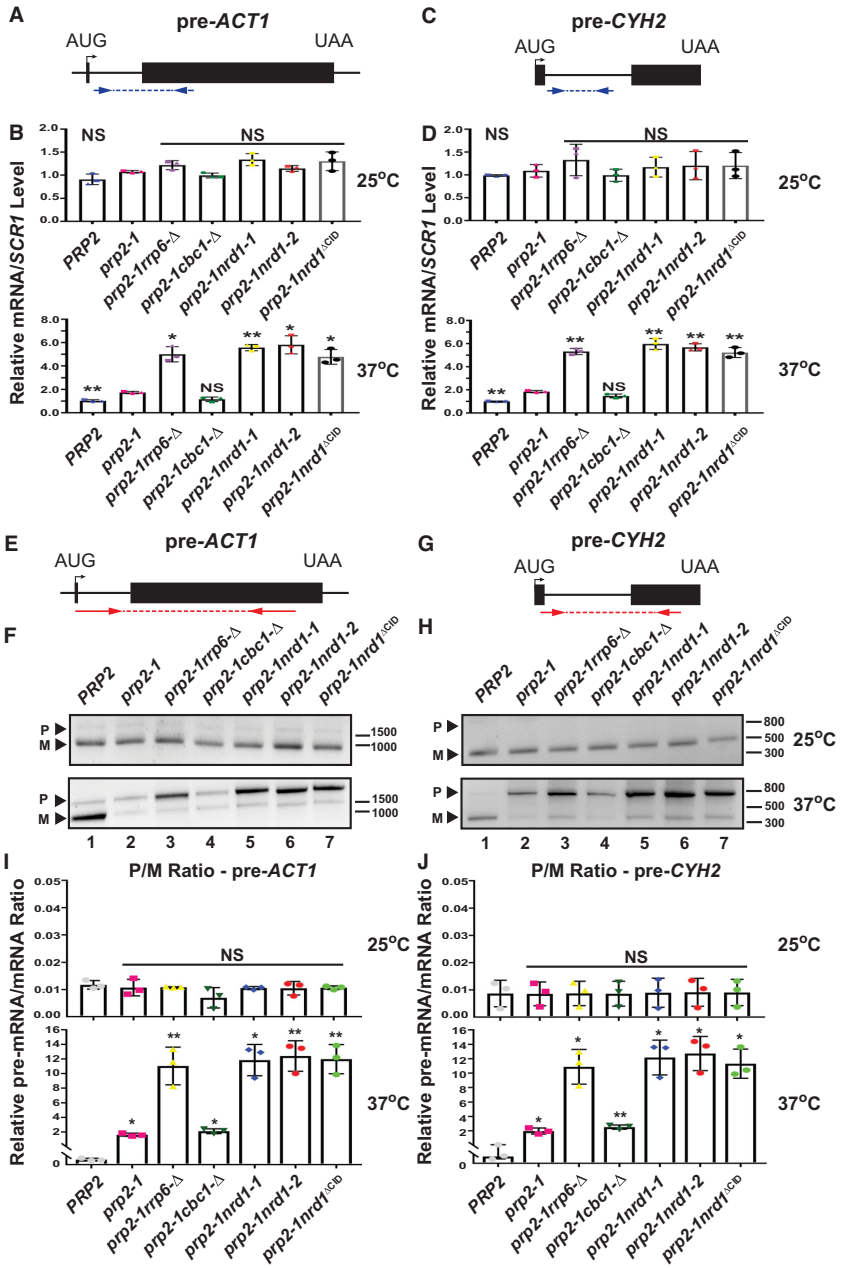

Figure 2. Nrd1p facilitates the degradation of aberrant mRNPs generated in splice-defective (*prp2-1*) yeast strains. (**A**–**D**) Relative abundance of two intron-containing precursor pre-*ACT1* (B) and pre-*CYH2* (D) mRNAs at permissive (25°C) and non-permissive (37°C) temperature in the *PRP2*$^{+}$, *prp2-1* and their isogenic derivative strains as determined by qRT-PCR using a primer set encompassing the blue amplicons located within the intronic regions of each gene (indicated in top cartoons). The normalized value of each pre-mRNA signal from *PRP2*$^{+}$ strains was set to 1. *P*-value was estimated with respect to the steady-state levels of the transcript in the *prp2-1* strain at each temperature. Three independent samples of random-primed cDNA (from biological replicates, $N = 3$) were prepared from indicated strains, pre-grown at 25°C followed by a 3-h shift of the yeast strains at 37°C before being subjected to qRT-PCR. Transcript copy numbers/50 ng cDNA for *prp2-1* strains were normalized to *SCR1* RNA signals obtained from respective samples and are shown as means ± SE. *P*-values were estimated from the Student's two-tailed *t*-test for a given pair of test strains for each message and are presented with the following symbols, $*P < 0.05$, $**P < 0.005$ and $***P < 0.001$, NS, not significant. (**E**–**H**) Relative steady-state levels of precursor and mature forms of *ACT1* and *CYH2* mRNAs at 25°C and 37°C temperature in the *PRP2*$^{+}$, *prp2-1,* and their isogenic derivative strains. Representative gel showing the relative levels of the precursor as well as mature pre-*ACT1* (**F**) and pre-*CYH2* mRNA (**H**) in these strains as determined by the semi-quantitative end-point PCR reactions carried out using the primer sets locating within the exon1 and exon2 of each gene encompassing the red amplicons (indicated on top of each graph). Positions of the relevant size standards are shown on the right side of each gel panel. Note that the primer sets used in the experiments could detect both the pre-mRNAs and their mature forms and thus enabled us to specifically and precisely estimate both the precursor and mature forms of these mRNAs. (**I** and **J**) Quantification of the semi-quantitative PCR data from (**F**) and (**H**) showing the relative levels of the pre-mRNAs and mRNAs of *ACT1* and *CYH2* mRNAs presented in the ratio of precursor to mature form of each RNA at 25 and 37°C. The steady-state intensity for each of the mature and precursor forms of each RNA was derived from three independently prepared gels normalized to the intensity of *SCR1* mRNAs (not shown). The ratio of precursor to mature species was determined and presented as mean P/M ratio ± SE. *P*-values were estimated from the Student's two-tailed *t*-test for a given pair of test strains for P/M values for each RNA and are presented with the following symbols, $*P < 0.05$, $**P < 0.005$ and $***P < 0.001$, NS, not significant.

sor mRNAs showed a dramatic steady-state enhancement of approximately three folds in *prp2-1 nrd1-1*, *prp2-1 nrd1-2* and *prp2-1 nrd1*Δ^{CID} strains at the non-permissive temperature of 37°C (Figure 2B and D, bottom histograms). This finding thus strongly indicates that Nrd1p promotes the degradation of the intron-containing precursor forms of these RNAs in *prp2-1* strain at the non-permissive temperature of 37°C. Despite being produced in extremely low abundance at permissive temperature of 25°C in all of these isogenic strains, we did not observe any substantial alteration in the steady-state levels of these precursor transcripts in these strains at 25°C (Figure 2B and D, top histograms). Furthermore, as before, both pre-*ACT1* and pre-*CYH2* RNA transcripts displayed a comparable stabilization in *prp2-1 rrp6*-Δ strain to that exhibited in *nrd1* mutant strains while not exhibiting any stabilization in *prp2-1 cbc1*-Δ strain at 37°C (Figure 2B and D, bottom histograms).

To further corroborate our finding, we repeated the same experiment with an alternative approach by performing the end-point PCR with a different set of primer specific for *ACT1* and *CYH2* gene sequences in which the sense and antisense primers are located on exons 1 and 2, respectively (Figure 2E and G, Supplementary Table S4). An end-point PCR using these primer sets specific for *ACT1* and *CYH2* exons followed by the analysis of the PCR product by the gel electrophoresis yielded two bands – one each for the precursor (P) and mature (M) messages (Figure 2F and H). Analysis of steady-state profiles of the precursor and mature messages of *ACT1* and *CYH2* RNA from these strains at 25 and 37°C revealed that the pre-*ACT1* and pre-*CYH2* mRNAs generated at 25°C in all the isogenic strains were barely detectable relative to their mature forms (Figure 2F and H, top panels). In contrast, the precursor messages for both the RNAs at 37°C were fairly strong in *prp2-1* and its isogenic exosome and *nrd1* deficient strains (Figure 2F and H, bottom panels). Consistent with the data observed from the experiments presented in Figure 2A–D, the pre-mRNA species of both the *ACT1* and *CYH2* genes displayed more intense bands in *prp2-1 nrd1-1*, *prp2-1 nrd1-2*, *nrd1*Δ^{CID} and *prp2-1 rrp6*-Δ strains relative to *prp2-1* strain at 37°C (Figure 2F and H, bottom panels). As observed before, the *prp2-1 cbc1*-Δ strain did not exhibit any enhancement in the intensity of the precursor RNA species (Figure 2F and H, bottom panels) (12). Further quantification of these observed bands of precursor and mature species of the *ACT1* and *CYH2* RNA yielded a low ratio of precursor to mature species (P/M ratio) for all the strains at the permissive temperature of 25°C (Figure 2I and J, top histograms). In contrast, the P/M ratio for both the RNA species in *prp2-1 rrp6*-Δ, *prp2-1 nrd1-1*, *prp2-1 nrd1-2* and *prp2*-1 *nrd1*Δ^{CID} strains was found to be approximately 12-fold higher relative to the value observed in *prp2-1* and *prp2-1 cbc1*-Δ strains at the non-permissive temperature of 37°C (Figure 2I and J, bottom histograms). Together, these data strongly support the conclusion that the mutations in the *NRD1* gene dramatically stabilized the steady-state levels of both the representative intron-containing precursor RNA species, thereby signifying that Nrd1p (and perhaps NNS complex) facilitates rapid exosomal degradation of these representative splice defective RNAs.

Nrd1p plays a vital role in the degradation of aberrantly long 3′-extended mRNAs produced in the '3′-end processing defective' *rna14-1* yeast strain

In the conditionally lethal 3′-end processing-defective *rna14-1*/*rna15-2* strains, faulty transcripts are produced globally at the restrictive temperature of 37°C that harbor aberrantly long 3′-extended read-through termini (68–71). The nuclear exosome was found to processes these defective transcripts to their natural length (61,72). Consequently, they are stabilized by the mutations in the components of either the nuclear exosome, TRAMP or CTEXT (12). These data collectively suggest that aberrantly long transcripts with 3′-extended read-through termini in *rna14-1* strains undergo massive degradation in an exosome/TRAMP/CTEXT-dependent manner. Having demonstrated that Nrd1p promotes the decay of aberrant transcription-assembly defective and splice-defective messages, we went ahead to evaluate the role of Nrd1p in the decay of the aberrantly long 3′-end-extended transcripts. We examined if the decay of aberrantly long 3′-extended read-through forms of two arbitrarily chosen model mRNAs, *LYS2* and *CYC1* (12), were affected by the *nrd1* mutations. These two transcripts were selected based on differences in their length—mature *LYS2* mRNA being 4.18 kb and mature *CYC1* mRNA being 0.63 kb long. Transcripts of such diverse ranges were chosen to evaluate if the impact of the Nrd1p (and NNS complex) is similar and comparable on long and short messages (12). Moreover, in addressing the impact of NNS complex on these aberrant 3′-end processing defective RNAs, we deliberately selected qRT-PCR as a method of choice over northern blot analysis for the following reason. A typical northern blot using the total RNA samples extracted from *rna14-1* strain at 37°C, when probed against a specific transcript, yields a signal consisting of really long smear trailing behind the particular band of the mature length of that RNA (instead of a sharp band at the mature position). The smear results from differential migration of the heterogeneous population of messages with variable extensions at the 3′-termini during the initial fractionation by gel electrophoresis (61,72). Consequently, the abundance of these transcripts is impossible to quantify precisely from the northern blot using the standard image analysis tools. In contrast, the use of qRT-PCR using a primer set spanning defined regions downstream of *LYS2* and *CYC1* genes (see cartoon in Figure 3G and H and Supplementary Table S4) would lead to the precise determination of the abundance of a specific aberrant read-through transcript (*LYS2* or *CYC1*) of a defined length in a selective fashion from the heterogeneous population of the extended species. The goal mentioned above would thus be achieved by using two primer sets defining the amplicons C_{EXQ} (*CYC1*-extended) and L_{EXQ} (*LYS2* –extended), respectively, for the qRT-PCR assay (Primer information given in Supplementary Table S4). These amplicons span the further downstream region from the polyadenylation sites (3200 nt for *LYS2* and 1861 nt for *CYC1* from respective translation termination codons) (Figure 3G and H, shown by blue lines). In addition, the use of alternative primer sets spanning within the mature/coding regions of these genes defining the amplicons C_{MQ} and L_{MQ} respec-

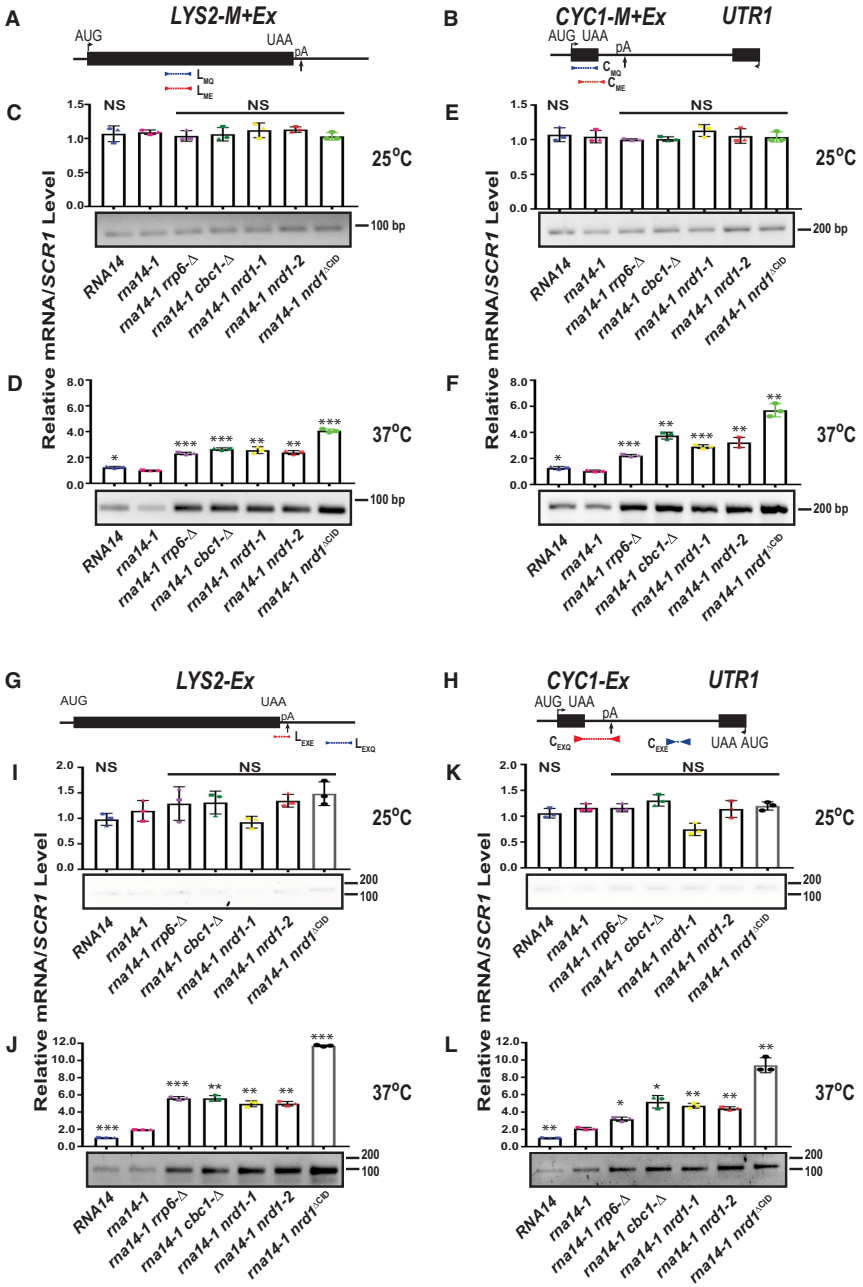

Figure 3. Nrd1p promotes the degradation of aberrant mRNPs produced in the 3′-end processing-defective (*rna14-1*) yeast strains (**A** and **B**). Cartoons showing the coding and downstream regions of the *LYS2* and *CYC1* gene and the position of the primer-sets and amplicons used in the experiments presented in panels (**C**–**F**). Relative abundance of two mature (and 3′-extended forms, if any), *LYS2-M* (**C-D**) and *CYC1-M* (**E** and **F**) forms of these RNAs at permissive (25°C) and non-permissive (37°C) temperature in the *RNA14*$^{+}$, *rna14-1* and their indicated isogenic derivative strains. In each panel, the top histograms depict the levels of mature (and extended, if any) species of these RNAs quantified by qRT-PCR, and the bottom gels show their levels detected by end-point PCR. Note that the primer sets used in these qRT- and end-point PCR reactions are located within the coding region of each gene (shown in blue and red lines respectively for amplicons used in qRT- and end-point PCR in A and B). Three independent samples of random-primed cDNA (from biological replicates, $N = 3$) were prepared from indicated strains, pre-grown at 25°C followed by a 3-h shift of the yeast strains at 37°C before being subjected to either qRT-PCR or end-point PCR analysis. Transcript copy numbers/3 ng for *RNA14*, *rna14-1,* and their derivative strains were normalized to *SCR1* RNA signals obtained from respective samples and are shown as means ± SE. The normalized value of a specific RNA signal from the *RNA14*$^{+}$ sample was set to 1. *P*-values were estimated from the Student's two-tailed *t*-test for a given pair of test strains for each message and are presented with the following symbols, $*P < 0.05$, $**P < 0.005$ and $***P < 0.001$, NS, not significant. *P*-value was estimated with respect to the normalized steady-state levels of the transcript in the *rna14-1* strains at each temperature. (**G** and **H**). Cartoons showing the coding and downstream regions of the *LYS2* and *CYC1* gene and the position of the primer-sets and amplicons used in the experiments presented in panels (**I–L**). (**I**–**L**) Relative abundance of 3′-extended forms of *LYS2* (**I** and **J**) and *CYC1* (**K-L**) RNAs determined either by the qRT-PCR (top histogram) or by end-point PCR (bottom gels). These reactions were carried out using primer sets that encompass either specifically the 3′-extended region (blue amplicons in **G** and **H**) or both the coding and downstream region (red amplicons in **G** and **H**) of each gene. These primer sets will specifically amplify the 3′-extended read-through transcripts and thus enable us to specifically and precisely estimate only their 3′-extended forms. Except for the use of primer sets, all other experimental parameters and procedures were kept the same as that described for experiments depicted in panels **E** and **F**.

tively (Figure 3A and B, shown by blue lines, Supplementary Table S4) would amplify only the mature transcript at both the permissive and the non-permissive temperature in *RNA14*$^+$ strain. In contrast, they would amplify only mature transcripts at permissive temperature and a pool of mature and extended transcripts at a non-permissive temperature in *rna14-1* strain.

To ensure that the selected primer sets yield products according to our expectations, we first evaluate the relative levels of mature (using L_{MQ} and C_{MQ}) and the extended transcripts (using L_{EXQ} and C_{EXQ}), of the *LYS2* and *CYC1* RNAs in *RNA14*$^+$ and *rna14-1* strains. As shown in Supplementary Figure S1A,B, at the permissive temperature of 25°C, the levels of extended transcripts for both *LYS2* and *CYC1* RNA species are much lower than the mature species in both *RNA14*$^+$ and *rna14-1* strains (≈10% of the mature species). Similar profiles of mature and extended species of both the RNA species were also observed in *RNA14*$^+$ strain at the non-permissive temperature of 37°C. This distribution of the mature and extended species was in perfect agreement with the expectation, since at 25°C in both strains and at 37°C in *RNA14*$^+$ strain the amount of the extended species would be negligibly small (Supplementary Figure S1A,B). In contrast, in the *rna14-1* strain at 37°C the abundance of the extended species is very high relative to the other conditions (Supplementary Figure S1A,B). Although the predicted levels of mature species of both the *LYS2* and *CYC1* RNAs in the *rna14-1* strain were relatively low at 37°C, the transcripts for both the RNAs were substantially high due to the cumulative amplification of mature and extended species together. These data corroborated our assumption and justified using the amplicons, $C_{MQ}/C_{EXQ,}$ and L_{MQ}/L_{EXQ} to determine the abundance of the 3′-extended read-through transcripts of these model RNAs in *rna14-1* (and its *nrd1* derivative strains).

Next, we estimated both the mature/'mature + extended' and the extended read-through transcripts of *LYS2* and *CYC1* RNAs in the *RNA14*$^+$, *rna14-1* and its *nrd1-1*, *nrd1-2,* and *nrd1*Δ^{CID} derivative strains at both the permissive and non-permissive temperature of 25°C and 37°C using both the primer sets defining the amplicons L_{MQ}/L_{EXQ} and C_{MQ}/C_{EXQ}. The results are presented in Figure 3C–F (using amplicons L_{MQ} and C_{MQ}) and Figure 3I-L (using amplicons L_{EXQ} and C_{EXQ}). As expected, the abundance of these mRNAs was very similar in all the strains at 25°C using both sets of amplicons (Figure 3C–E, I–K). The similarity in their levels at 25°C presumably resulted from the predominant production of mature species only, using both of these primer sets that are not affected by the presence or absence of functional Nrd1p. Predictably, when using amplicons L_{MQ} and C_{MQ} in *RNA14*$^+$ and *rna14-1* strains at 37°C, the abundance of both the *LYS2* and *CYC1* is similar and comparable (Figure 3D–F, first two histogram bars). In contrast, the L_{EXQ} and C_{EXQ} amplicons revealed higher levels of the extended read-through versions of the *LYS2* and *CYC1* RNAs in *rna14-1* strains at 37°C (Figure 3J–L, first two histogram bars). Most significantly, regardless of the amplicons used, the steady-state levels of both the 'mature + extended' (with L_{MQ} and C_{MQ}) and extended (with L_{EXQ} and C_{EXQ}) forms of *LYS2* and *CYC1* mRNAs were found to be substantially enhanced in the yeast strains harboring mutant alleles of *NRD1* (Figure 3D–F and J–L). As noted before (12), these extended RNA species were also stabilized by *rrp6*-Δ and *cbc1*-Δ alleles. Notably, a comparison of RNA stabilizations between that found with amplicons L_{MQ} and C_{MQ} (Figure 3D–F) and that obtained with amplicons L_{EXQ} and C_{EXQ} (Figure 3J–L) in *rna14-1 nrd1* mutants relative to *rna14-1* revealed that stabilizations obtained with amplicons L_{MQ} and C_{MQ} are more robust and dramatic. These data suggest that the greater extent of stabilizations in *rna14-1 nrd1* strains found with L_{EXQ} and C_{EXQ} is due to selective enrichment of only the extended read-through transcripts of these RNAs. In contrast, their relatively lower abundance in *rna14-1 nrd1* strains with L_{MQ} and C_{MQ} resulted from contamination of their mature species in the population of extended forms. We further corroborated this observation by repeating the experiments with a different set of primers defining the amplicons L_{ME}/C_{ME} and L_{EXE}/C_{EXE} (Figure 3G and H) using end-point PCR reaction (see Supplementary Table S4), which revealed a similar extent of enhancement of steady-state levels of the aberrant read-through transcripts in *rna14-1 nrd1-1*, *rna14-1 nrd1-2* and *rna14-1 nrd1*Δ^{CID} strains at 37°C (gel panels at the bottom of each histogram in Figure 3D–F and J–L) but not at 25°C (gel panels at the bottom of each histogram in Figure 3C–E and I–K). These findings support the conclusion that Nrd1p (and NNS complex) promotes the nuclear decay of the abnormally long 3′-extended version of the model *LYS2* and *CYC1* mRNAs generated in the *rna14-1* strain at 37°C.

Steady-state enhancement of the model test mRNAs is directly associated with their diminished decay in *hpr1*-Δ*nrd1*, *prp2-1 nrd1* and *rna14-1 nrd1* strains relative to *hpr1*-Δ, *prp2-1* and *rna14-1* strains

To further corroborate if the enhancement of the steady-state levels of these transcripts in various *nrd1* mutant strains is linked to their decay, the decay rates of these faulty messages were determined in wild-type and different *nrd1* strain backgrounds. The decay rates of these selected mRNAs were determined post 2 to 3 h of the shift from 25 to 37°C of the growing yeast cultures followed by the block of RNAPII transcription by 1,10-phenanthroline. Subsequent determination of steady-state levels of these faulty transcripts at different times by qRT-PCR was carried out using the same sets of primers as in the previous experiments. As shown in Figure 4, decay rates of all of the aberrant forms of transcription elongation-defective *ACT1-Tad* and *CYC1-Tad* mRNAs (Figure 4A and B), precursor forms of the splice defective pre-*CYH2* mRNA (Figure 4C), and the faulty read-through transcripts of *LYS2-Ex* and *CYC1-Ex* mRNAs (Figure 4D and E) were significantly diminished in *nrd1-1*, *nrd1-2* and *nrd1*Δ^{CID} strains in comparison to that in the corresponding wild-type strains with the concomitant increase in their half-life values (Table 2). These findings are consistent with the conclusion that all the tested representative transcription-elongation/assembly-defective, splice-defective, and aberrantly long read-through transcripts with 3′-extensions are subject to nuclear degradation dependent on Nrd1p.

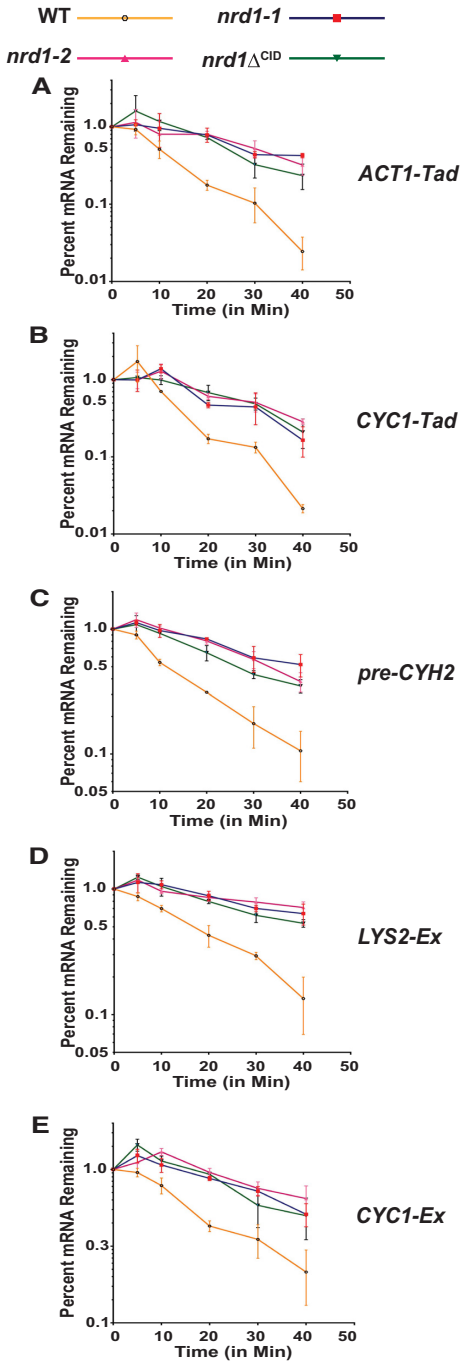

Figure 4. Decay kinetics of representative transcription-elongation-defective *ACT1-Tad* and *CYC1- Tad* (**A** and **B**), splice-defective pre-*CYH2* (**C**), aberrantly long 3′-end processing-defective *LYS2-Ex* and *CYC1-Ex* (**D** and **E**) mRNAs at 37°C in the wild-type (orange line) and yeast strains harboring *nrd1-1* (blue line), *nrd1-2* (pink line), and *nrd1*Δ^{CID} (green line) mutations. Decay rates were determined by qRT-PCR analysis from three independent samples of 3 ng cDNA (50 ng for pre-*ACT1* and pre-*CYH2* mRNAs) (biological replicates, $N = 3$) extracted from yeast strains harvested at various times following the treatment of the cells with transcription-inhibitor 100 μg/ml 1, 10-phenanthroline. qRT-PCR signals were normalized to *SCR1* RNA signals obtained from the same cDNA samples, and the normalized signals (mean values ± SD from three biological replicates, $N = 3$) from each time point were presented as the fraction of remaining RNA (with respect to normalized signals at 0 min, which was set to 1) as a function of time of incubation in the presence of 1,10-phenanthroline.

nrd1 mutations do not cause any steady-state enhancement of any model test mRNAs in any of the *HPR1*$^+$, *PRP2*$^+$ and *RNA14*$^+$, nor do they cause any alterations in the cellular levels of the nuclear exosome, TRAMP and CTEXT components

An alternative explanation for our findings would be that Nrd1 defects specifically increase the levels of the normal forms of our test mRNAs. This possibility is ruled out by the fact that the levels of these transcripts (*ACT1, CYC1, CYH2* and *LYS2*) are unchanged in the *rrp6*-Δ, *cbc1*-Δ, and all of the *nrd1* mutant strains in the *HPR1*$^+$, *PRP2*$^+$ and *RNA14*$^+$backgrounds (Supplementary Figure S1C–E). Likewise, we ruled out the possibility that the stabilization of various aberrant mRNAs by *nrd1* mutations is an indirect effect of down-regulation of the components of the nuclear exosome, TRAMP or CTEXT. Measurements of the levels of mRNAs encoding these components (Supplementary Figure S2A–C) and their protein levels (Supplementary Figure S2D) show no changes in the *nrd1* mutants compared to wild-type. The results of these control experiments support our conclusion that Nrd1 directly destabilizes the aberrant forms of these transcripts.

Stabilization of export-defective messages requires Nrd1p but not its C-terminal domain

In yeast, a variety of nucleus-retained, export deficient mRNAs are generated during the terminal phase of the mRNP biogenesis and are classified into three different categories: (i) those that are generated due to *cis*-acting mutations in their transcript body (i.e. *lys2-187* mRNA) (15), (ii) global poly(A)$^+$ messages retained in the nucleus of the temperature-sensitive *nup116*-Δ mutant yeast strain (14) at the restrictive condition of 37°C due to a complete block of nuclear export (73) and (iii) naturally occurring nucleus-retained export-deficient non-aberrant messages (dubbed special messages) (24) (Table 1). Our previous work established that all of these messages undergo active nuclear degradation by the exosome and its cofactor CTEXT without any participation of TRAMP (12). An assessment of the functional role of the Nrd1p in the decay of export-deficient messages revealed that they were stabilized in *nrd1-1* and *nrd1-2* strain backgrounds (Figures 5 and 6). The destabilization of *lys2-187* mRNA at 25°C (Figure 5B), nucleus-arrested *ACT1* and *CYC1* mRNAs in *nup116*-Δ strains at 37°C (Figure 5E and G) and four export-incompetent special mRNAs *IMP3, SKS1, NCW2* and *GIC2* at 25°C (Figure 6C–F) were all rescued in *rrp6*-Δ, *cbc1*-Δ, *nrd1-1* and *nrd1-2* mutant isogenic yeast strains. As expected, normal export-efficient *CYC1* mRNA at 25°C (Figure 5A), *ACT1* and *CYC1* mRNA in *nup116*-Δ strains at 25°C (Figure 5D and F), and *CYC1* and *ACT1* in the normal background (Figure 6A and B) were unaffected by the *nrd1* mutations. Surprisingly and remarkably, none of the export-defective test messages displayed any steady-state enhancement in *nrd1*Δ^{CID} mutant isogenic strain (Figures 5 and 6). Likewise, the *nrd1*Δ^{CID} mutation did not suppress the mRNA accumulation defect caused by the *lys2-187* mutation, in contrast to suppression of the defect by the *nrd1-1* and *nrd1-2* mutations (Figure 5C). Consistent with this finding, *nrd1-1* and *nrd1-2* mutations suppressed the rapid decay of the

Table 2. Half-life values of various aberrant mRNAs in different yeast strains carrying various mutant alleles in *NRD1* gene in the backgrounds of transcription-elongation-defect (*hpr1*-Δ), splicing-defect (*prp2-1*) and 3′-end formation (*rna14-1*) defect.

		Half-life (in minutes) of specific target messages in various *nrd1* mutant strains			
Yeast strain defective in	Target aberrant message	Wild-type	*nrd1-1*	*nrd1-2*	*nrd1*Δ^{CID}
Transcription-elongation (*hpr1*-Δ)	*ACT1*	10.37	20.6	20.15	29.19
	CYC1	10.22	29.94	19.77	29.96,
Splicing (*prp2-1*)	pre-*CYH2*	9.925	20.15	20.09	19.85
3′-end Processing (*rna14-1*)	*LYS2*	10.24	20.06	19.75	19.86
	CYC1	10.37	20.06	20.15	29.19
None	*NCW2*	10.11	19.82	19.87	9.952

NCW2 message, while the *nrd1*Δ^{CID} mutation had no effect (Table 2 and Supplementary Figure S3A). The fact that the *nrd1*Δ^{CID} mutation does not suppress the rapid degradation of *NCW2* mRNA and other export defective messages in general suggests that Nrd1p does not require its CID domain for targeting export-deficient mRNAs for nuclear decay (Figures 5B,E,G, 6C–F).

Next, we established genetic epistasis between the Rrp6p, Cbc1p, and Nrd1p to confirm that the core exosome, CTEXT, and NNS complex collectively act as a part of the same pathway. Findings from this experiment revealed that steady-state levels of the two special messages, *NCW2* and *SKS1* observed in the single mutant *rrp6*-Δ, *cbc1*-Δ and *nrd1-2* strains, were not changed in the double mutant *rrp6*-Δ *nrd1-2*, *cbc1*-Δ *nrd1-2* strains (Figure 7B and C). Finally, we verified that all components of the NNS complex participate in the degradation of export-defective transcripts by demonstrating that their steady-state levels were dramatically stabilized in the yeast strains carrying *nab3-10* (Figure 7D–G) and *sen1-1* (Figure 7H–K) mutations relative to wild-type strain. The normal *CYC1* mRNA, in contrast, neither displayed any destabilization nor stabilization in any of these strains (Figure 7A, D, H). These data are thus consistent with the conclusion that Nrd1p-Nab3p-Sen1p together plays a crucial functional role in the decay of export defective special messages. Collectively, the findings from the experiments presented in this section strongly suggest that the Nrd1p-Nab3p-Sen1p complex plays a pivotal role in the nuclear degradation of representative aberrant nuclear mRNAs, which belong to diverse faulty messages (Table 3).

Strikingly, the *nrd1*Δ^{CID} mutation, unlike the *nrd1-1* and *nrd1-2* mutations, caused differential specificity towards the aberrant nuclear transcripts. While a dramatic effect of the *nrd1*Δ^{CID} mutant was observed in stabilizing the transcription/assembly-, splice- and 3′-processing-defective mRNAs (Figures 1–4), no stabilizing influence of this mutant was noted in case of export defective messages (Figures 5 and 6) (Table 3). This observation suggests that Nrd1p CID is required for targeting the aberrant messages produced in the early and intermediate stages of mRNP biogenesis but is unnecessary to promote the rapid decay of the export-incompetent messages. Since the interaction of Nrd1p-RNAPII in the *nrd1*Δ^{CID} strain is abolished (18,20,30,33,74), the findings described above suggest that the degradation of aberrant mRNAs generated during the early and intermediate mRNP biogenesis stage requires the Nrd1p complex to be recruited co-transcriptionally onto these transcripts via RNAPII-CTD. In contrast, the CID domain appears dispensable for the rapid degradation of export-defective messages, leading to the conclusion that Nrd1p supports the nuclear decay of the aberrant export-incompetent messages in an RNAPII-CTD independent manner.

RNAPII-dependent co-transcriptional recruitment of Nrd1p is vital for the exosome/TRAMP-dependent decay of the aberrant mRNAs derived during the early and intermediate stages of mRNA biogenesis

The observed requirement for the Nrd1 CID to target early and intermediate stage aberrant mRNAs for decay prompted us to test the hypothesis that Nrd1p is recruited co-transcriptionally on various kinds of aberrant transcripts. Consequently, the co-transcriptional recruitment profiles of Nrd1p on various messages were analyzed using the chromatin immunoprecipitation (ChIP) technique. Although the ChIP technique was thought to crosslink chromatin/DNA with the DNA-binding proteins, a vast majority of RNA binding proteins also crosslink to transcribing messenger RNAs, which remain physically associated with the chromatin. RNA-ChIP, adapted from the classical DNA-ChIP, is now widely used to study and analyze the binding profile of transcription, splicing, export and mRNA decay factors, which are recruited co-transcriptionally and remained strongly associated with the transcribing/maturing nascent mRNAs (75,76). Before carrying out the actual comparison of Nrd1p occupancy profile by RNA-ChIP, we first determined that the ChIP signal generated from our assay procedure is highly specific (Supplementary Figure S3B–E), which yields an Nrd1p occupancy profile that is consistent with previous reports (Supplementary Figure S7). Consequently, the co-transcriptional recruitment profiles of Nrd1p were determined on the *ACT1* and *CYC1* messages in *hpr1*-Δ mutant strains at 37°C were found to be dramatically higher than those estimated at 25°C (Figure 8A and B). Similarly, the Nrd1p occupancy of the export-incompetent *NCW2* mRNA was significantly higher than the typical export-efficient message *CYC1* (Figure 8C). These results support the hypothesis that Nrd1p (and NNS complex) is selectively recruited onto faulty and other target RNAs (such as special messages) in a co-transcriptional manner.

Next, we determined the Nrd1p recruitment profile onto the two representative model mRNAs from every class of aberrant messages in isogenic yeast strains carrying either

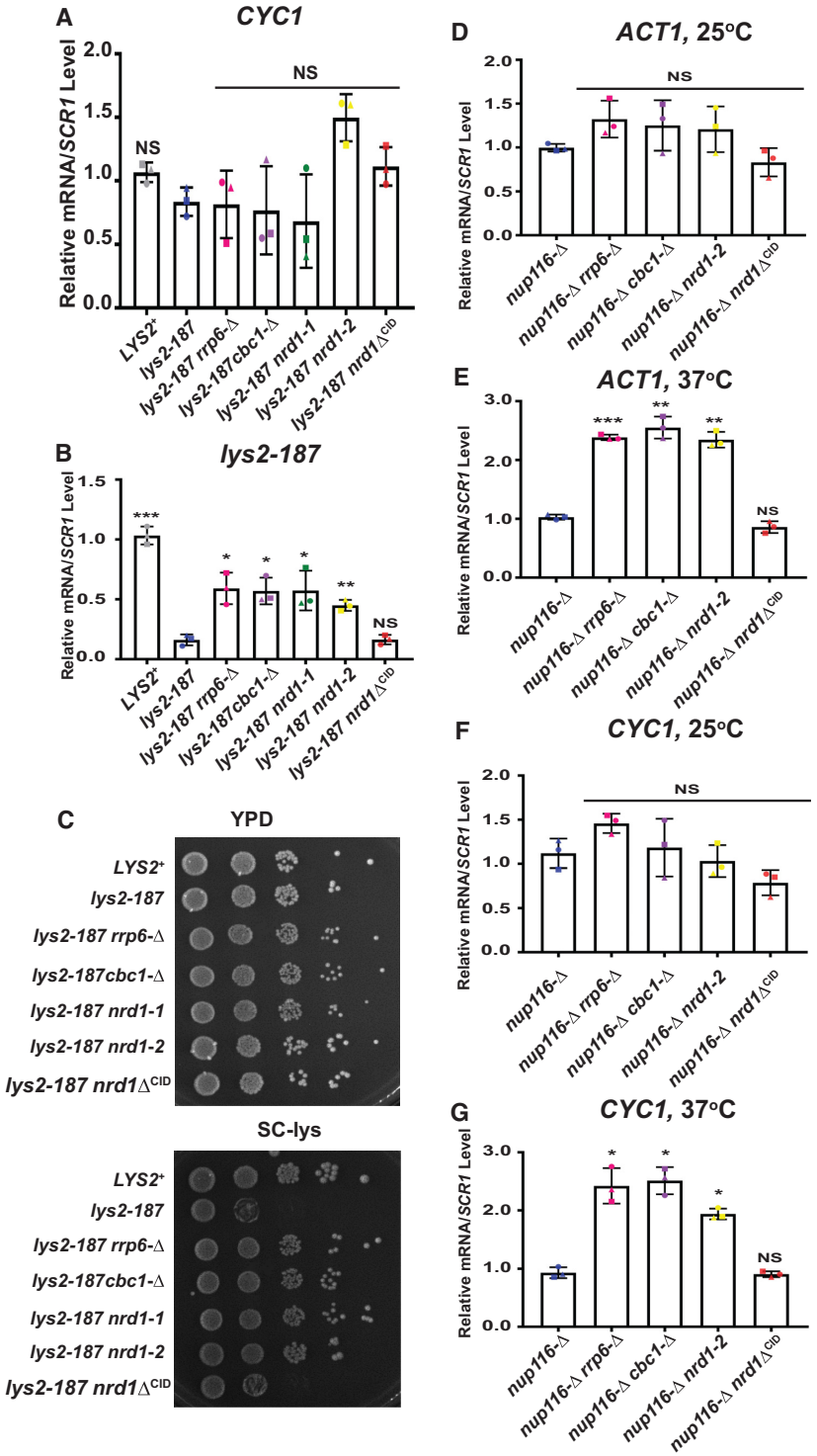

Figure 5. Rapid nuclear decay of export-defective messages is rescued by *nrd1-1* and *nrd1-2* mutations, but not by *nrd1*Δ^{CID} mutation. (**A** and **B**) Relative steady-state levels of export efficient normal *CYC1* (negative control) (A) and normal *LYS2* and export-defective *lys2-187* (B) mRNAs at 25°C in the indicated isogenic yeast strains. The normalized value of the *CYC1* and *LYS2* transcripts from the *LYS2*$^+$ sample was set to 1. *P*-value was estimated with respect to the steady-state levels of the respective transcripts in the *lys2-187* yeast strain (A and B). (**C**) Growth profile of *LYS2*$^+$ and the isogenic *lys2-187* mutant strains on YPD and SC-Lys medium at 25°C. A series of progressively diluted (1/10th) suspensions from the stock (concentration 10^5/cells per ml) of each strain were made, followed by spotting (10 μl) on YPD and lysine omission medium (SC-Lys). The plates were incubated at 25°C for 3–4 days before capturing the images. (**D**–**G**) Relative steady-state levels of nucleus-retained *ACT1* (D–E) and *CYC1* (F and G) at permissive (25°C) and non-permissive (37°C) in the *nup116*-Δ mutant and its various indicated isogenic strains. The normalized value of these transcripts from the *nup116*-Δ sample was set to 1. Transcript copy numbers/3 ng cDNA for *lys2-187* strains, copy numbers/2 ng cDNA of other strain backgrounds were normalized to *SCR1* RNA levels in respective samples and are shown as means ± SE. *P*-values estimated from the Student's two-tailed *t*-test for a given pair of test strains for each message are presented with the following symbols, $*P < 0.05$, $**P < 0.005$ and $***P < 0.001$, NS, not significant.

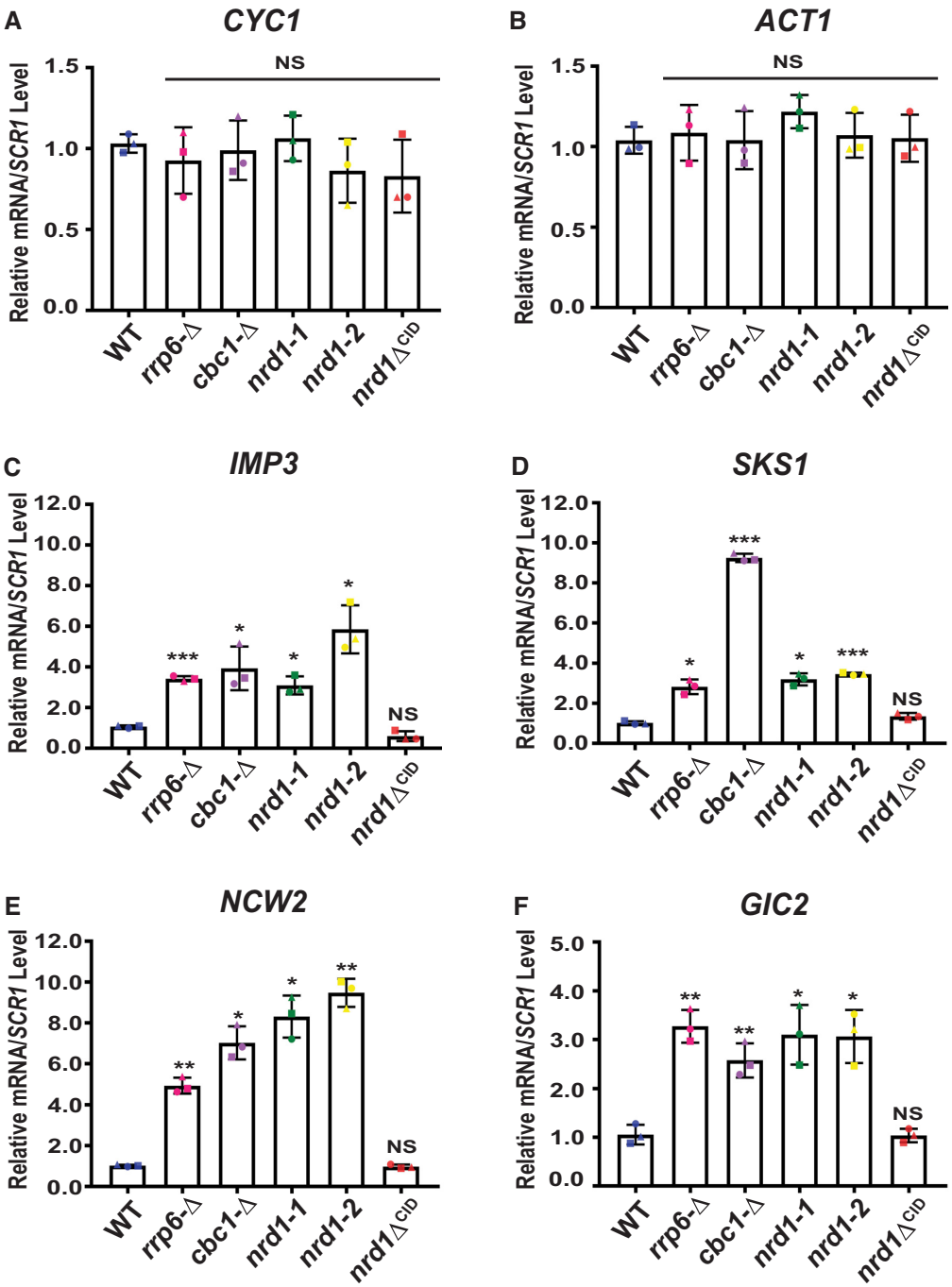

Figure 6. *nrd1-1* and *nrd1-2*, but not *nrd1*Δ^{CID} mutation rescue the rapid nuclear degradation of export-inefficient nucleus-retained special messages. (**A**–**D**) Relative steady-state levels of two export efficient mRNAs *CYC1* (A) and *ACT1* (B) and four export-inefficient special mRNAs, *IMP3* (C), *SKS1* (D), *NCW2* (**E**) and *GIC2* (**F**) at 25°C in a wild-type, *rrp6*-Δ, *cbc1*-Δ, *nrd1-1*, *nrd1-2* and *nrd1*Δ^{CID} strains. The normalized value of each specific mRNAs from the wild-type sample was set to 1. Three independent samples of random-primed cDNA (biological replicates, $N = 3$) samples were prepared from the indicated isogenic strains grown at 25°C before subjecting them to real-time qPCR analysis using primer sets specific for each mature mRNA. Transcript copy numbers/3 ng cDNA were normalized to *SCR1* RNA levels in respective samples and are shown as means ± SE. *P*-values estimated from the Student's two-tailed *t*-test for a given pair of test strains for each message are presented with the following symbols, $*P < 0.05$, $**P < 0.005$ and $***P < 0.001$, NS, not significant.

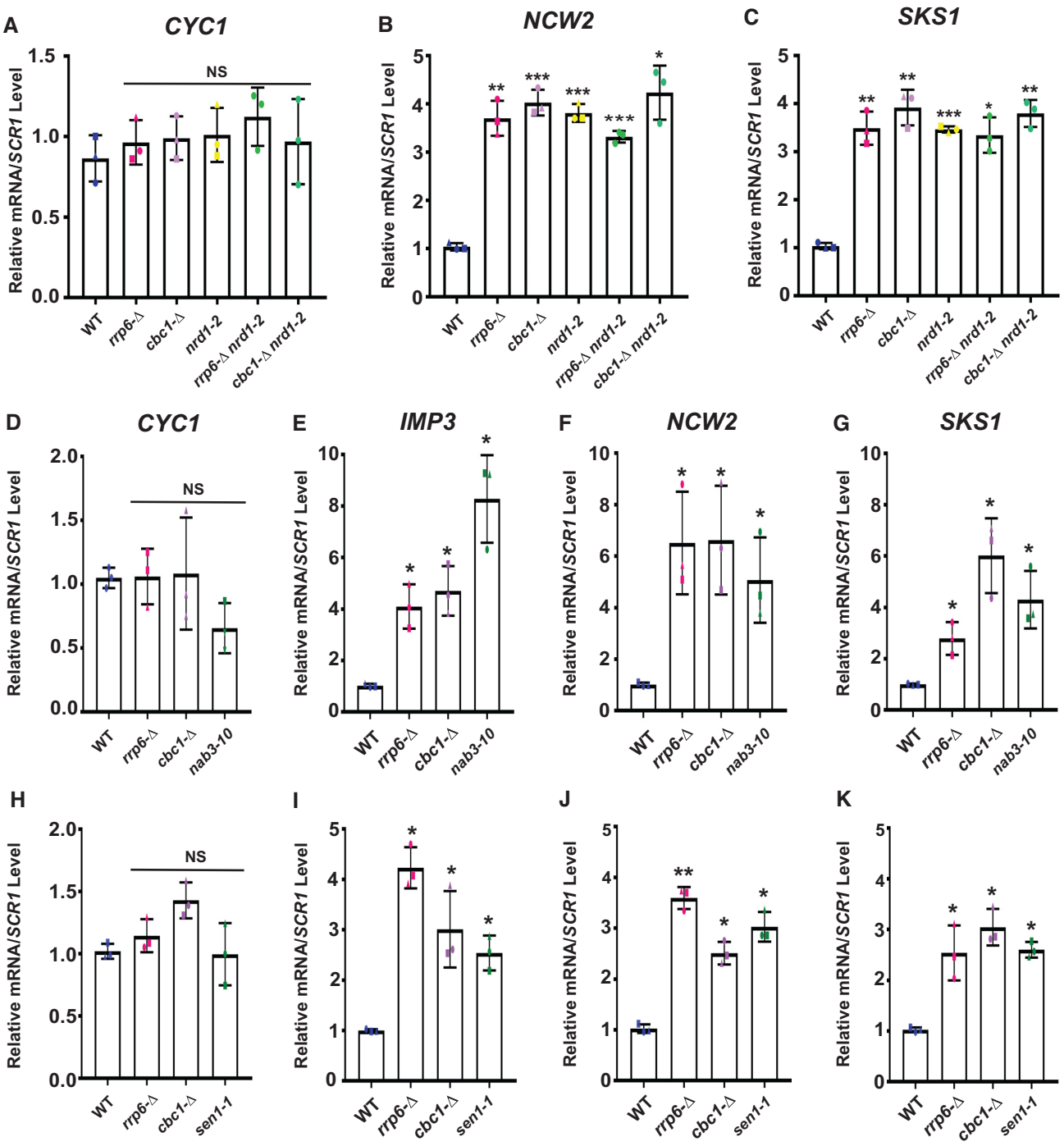

Figure 7. All the components of the NNS complex act together with the core nuclear exosome and CTEXT complex to facilitate the decay of the export defective special mRNAs. A-C. Relative steady-state levels of export efficient *CYC1* mRNA (**A**) and two export-inefficient special messages, *NCW2* (**B**) and *SKS1* (**C**) mRNAs at 25°C in an isogenic wild-type, *rrp6*-Δ, *cbc1*-Δ, *nrd1-2*, *rrp6*-Δ *nrd1-2* and *cbc1*-Δ *nrd1-2* strains. The normalized value of each specific mRNAs from the wild-type sample was set to 1. (**D–K**) Relative steady-state levels of normal export-efficient *CYC1* (D and H) and three export-inefficient special mRNAs, *IMP3* (E and I), *NCW2* (F and J) and *SKS1* (G and K) at 25°C in the indicated *nab3* (**D–G**) and *sen1* (**H–K**) isogenic yeast strain series. Normalized values of the transcript in the wild-type samples were set to 1. The RNA extraction and steady-state level of the specific mRNAs were determined as described in the legend of Figure 1. *P*-values were estimated from the Student's two-tailed *t*-test for a given pair of test strains for each message and are presented with the following symbols, $*P < 0.05$, $**P < 0.005$ and $***P < 0.001$, NS, not significant.

Table 3. Specificity of Nrd1p in the decay of various aberrant nuclear mRNA targets examined in this study and the effect of various *nrd1* mutants in their stabilization.

Stages of nuclear mRNP biogenesis	mRNP biogenesis event	Nature of aberrant mRNAs	Involvement of Nrd1p	Effects of different *nrd1* mutations in the stabilization of		
				nrd1-1	*nrd1-2*	*nrd1*Δ^{CID}
Early	Transcription	Transcription-elongation defective	+	+	+	+
	splicing	Splicing defective Intron-containing	+	+	+	+
Intermediate	3′-end processing	Aberrant transcription termination read-through transcripts with long 3′-Extension	+	+	+	+
Late	Nuclear export	Export Defective	+	+	+	–

an *NRD1*$^{+}$ or *nrd1*Δ^{CID} allele (Figure 8D–G). Our findings revealed that the representative transcription-elongation defective, splice defective and 3′-end processing-defective transcripts display a significantly higher occupancy of Nrd1p relative to that estimated in corresponding *nrd1*Δ^{CID} isogenic strains at the restrictive temperature of 37°C (Figure 8D–F). Furthermore, we also found that the low recruitment of Nrd1p observed in these *nrd1*Δ^{CID} strains was not associated with its low expression level, as shown by comparable Nrd1p expression levels in both *NRD1*$^{+}$ and *nrd1*Δ^{CID} yeast strains (Figure 8D–F). This observation indicated that Nrd1p occupancy on to the test mRNAs in an *nrd1*Δ^{CID} yeast strain is significantly lower because of its lower co-transcriptional recruitment, owing to the lack of association of N-terminally truncated nrd1Δ^{CID}p protein with the RNAPII-CTD. These findings support the view that Nrd1p recruitment to aberrant messages derived in the early and intermediate phase of mRNP biogenesis requires Nrd1p interaction with the RNAPII-CTD.

Nuclear degradation of export-defective aberrant mRNAs generated in the late phase of mRNP biogenesis requires Pcf11p-dependent recruitment of Nrd1p, which precedes the recruitment of the Rrp6p/nuclear exosome

Finally, we found that Nrd1p occupancy on two representative export-defective special messages, *NCW2* and *SKS1* mRNAs in the wild type and *nrd1*Δ^{CID} mutant yeast strains at 25°C, was very similar (Figure 8G). This observation strongly supports the view that Nrd1p recruitment on export-defective messages remains unaltered in an *nrd1*Δ^{CID} strain relative to wild type and is independent of the RNAPII. These collective findings from experiments described in previous and current sections suggest that Nrd1p (and NNS complex) participates in the nuclear degradation of all kinds of aberrant mRNA targets derived at various phases of mRNP biogenesis and its recruitment onto these aberrant messages is vital for their nuclear decay.

However, while the co-transcriptional recruitment of Nrd1p in the early/intermediate phase is strongly dictated by its interaction with RNAPII (via the interaction of the RNAPII CTD-Nrd1pCID domain), its recruitment onto the export-defective messages generated at the terminal phase of mRNP biogenesis is independent of RNAPII. To find out the cellular recruiter of Nrd1p onto the export-inefficient messages, we scrutinized the literature in search of an ideal factor, which should be characterized by its ability (i) to support only the decay of export-defective messages but not the decay of other aberrant classes, (ii) to selectively promote the recruitment of Nrd1p on the model-export defective messages only and (iii) to physically interact with Nrd1p.

Pcf11p, a key component of cleavage factor 1A (CF1A) involved in the transcription termination and cleavage/polyadenylation of poly(A)$^{+}$ RNAs, fits these criteria. Importantly, Pcf11p also possesses a CID (CTD-interacting domain) like Nrd1p, and it interacts with RNAPII and many nascent mRNAs after being recruited by RNAPII via its CID (77–81). Interestingly, Nrd1p and Pcf11p interact physically by affinity capture RNA method (44) and genetically by dosage rescue (82). Our initial effort to test the Pcf11p as the possible recruiter of Nrd1p revealed that a mutant yeast strain harboring a *pcf11-2* allele (77) did not enhance the steady-state levels of two representative transcription-elongation/assembly-defective messages in THO mutant isogenic strain background (Figure 9A). In contrast, the *pcf11-2* allele stabilized the two export-defective special messages, *NCW2* and *SKS1* mRNAs (Figure 9B), thereby strongly supporting our prediction. Consistent with this finding, a comparison of the Nrd1p occupancy profiles on the same group of representative messages revealed that, while recruitment profile on the transcription-elongation assembly defective *ACT1-Tad* and *CYC1-Tad* messages remained unaltered in *pcf11-2* mutant yeast strain, it is significantly reduced on the *NCW2* and *SKS1* mRNAs in the same *pcf11-2* strain (Figure 9C and D). This finding is thus consistent with the conclusion that Pcf11p plays a vital functional role in the co-transcriptional recruitment of Nrd1p onto the export-defective messages, thereby promoting their nuclear degradation by the nuclear exosome. Notably, Pcf11p is part of cleavage factor-1A (CF1A), a hexameric protein composed of two copies of each of Rna14p and Rna15p and one copy of each of Pcf11p and Clp1p (83). Interestingly, a mutation in any CF1A components led to the defect of the entire complex in the 3′-end cleavage and polyadenylation function, thereby supporting the argument that all of the four components of CF1A function collectively (80,84). Earlier evidence suggests that Pcf11p does not act independently of the CF1A complex (80,84). The involvement of Pcf11p in the nuclear decay processes of

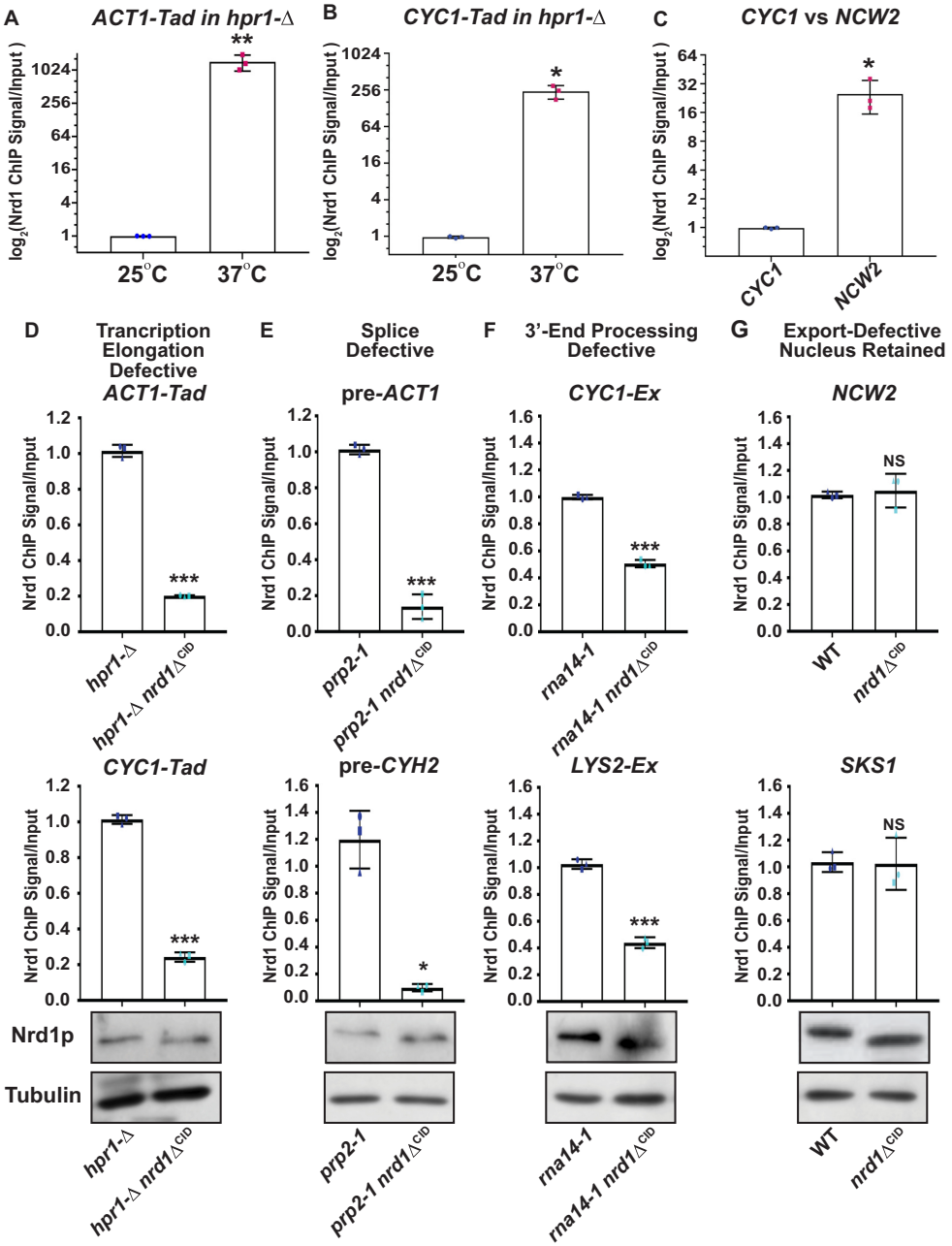

Figure 8. The co-transcriptional recruitment of Nrd1p lacking the *CID* domain is drastically impaired on transcription assembly-defective, splice-defective and 3′-extended aberrant messages compared to full-length Nrd1p but remains unaltered on export-defective special messages. (**A**–**C**) Nrd1p occupancy profiles of the transcription-assembly-defective *ACT1-Tad* (A) and *CYC1- Tad* (B) in an *hpr1*-Δ strain at 25 and 37°C, and a normal export efficient, *CYC1* and special *NCW2* mRNAs (C) in a wild-type yeast strain at 25°C. (**D**–**G**) Occupancy profile of full-length Nrd1p and Nrd1p lacking its *CID* domain on the (D) transcription assembly-defective *ACT1-Tad* and *CYC1-Tad* mRNAs at 37°C in isogenic *hpr1*-Δ and *hpr1*-Δ *nrd1*Δ*CID* strains, (E) intron-containing pre-*ACT1* and pre-*CYH2* at 37°C in isogeneic *prp2-1* and *prp2-1 nrd1*Δ*CID* strains, (F) 3′-extended read-through *CYC1-Ex* and *LYS2-Ex* transcripts at 37°C in *rna14-1* and *rna14-1 nrd1*Δ*CID* strains and (G) nucleus-arrested special messages *NCW2* and *SKS1* at 25°C in wild-type (*NRD1*$^{+}$) and *nrd1*Δ*CID* strains. Note that the quantification of the CYC1-Ex and LYS2 Ex messages by qRT-PCR at the final stage of the procedure was carried out using the primer-sets located in the 3′-extended region of these genes as described in Figure 3G–H. Panels at the bottom of each graph depict the expression levels of Nrd1p (both full-length and CID-deleted version) and tubulin as determined by western blot using anti-Nrd1p and anti-tubulin antibodies in each of the isogenic yeast strain series harboring either an *NRD1*$^{+}$ or a *nrd1*Δ^{CID} allele. Each lane contained an equal amount of quantified protein extracts from the indicated strains. A 70 and a 55 kDa band were detected in the extracts from the *NRD1* + and *nrd1*Δ^{CID} strains, respectively, with no non-specific band. For ChIP assays, fragmented and cross-liked chromatin preparation was conducted from indicated strains at a specific temperature from three independent biological replicates ($N = 3$) followed by the immunoprecipitation of the chromatin samples using a specific Nrd1p antibody. Immunoprecipitated DNA was recovered as mentioned in Materials and Methods section before qPCR analyses using the primer sets specific for the middle region of ORF (excluding Figure 8F) of each target mRNA. Mean normalized qPCR signals ± SD from the immunoprecipitated (output) DNA to the mean qPCR signal obtained from the total chromatin (input) DNA of each sample obtained from three experiments are presented Nrd1p ChIP Signal/Input. *P*-values estimated from Student's two-tailed *t*-tests for a given pair of test strains for each message are presented with the following symbols, $*P < 0.05$, $**P < 0.005$ and $***P < 0.001$, NS, not significant.

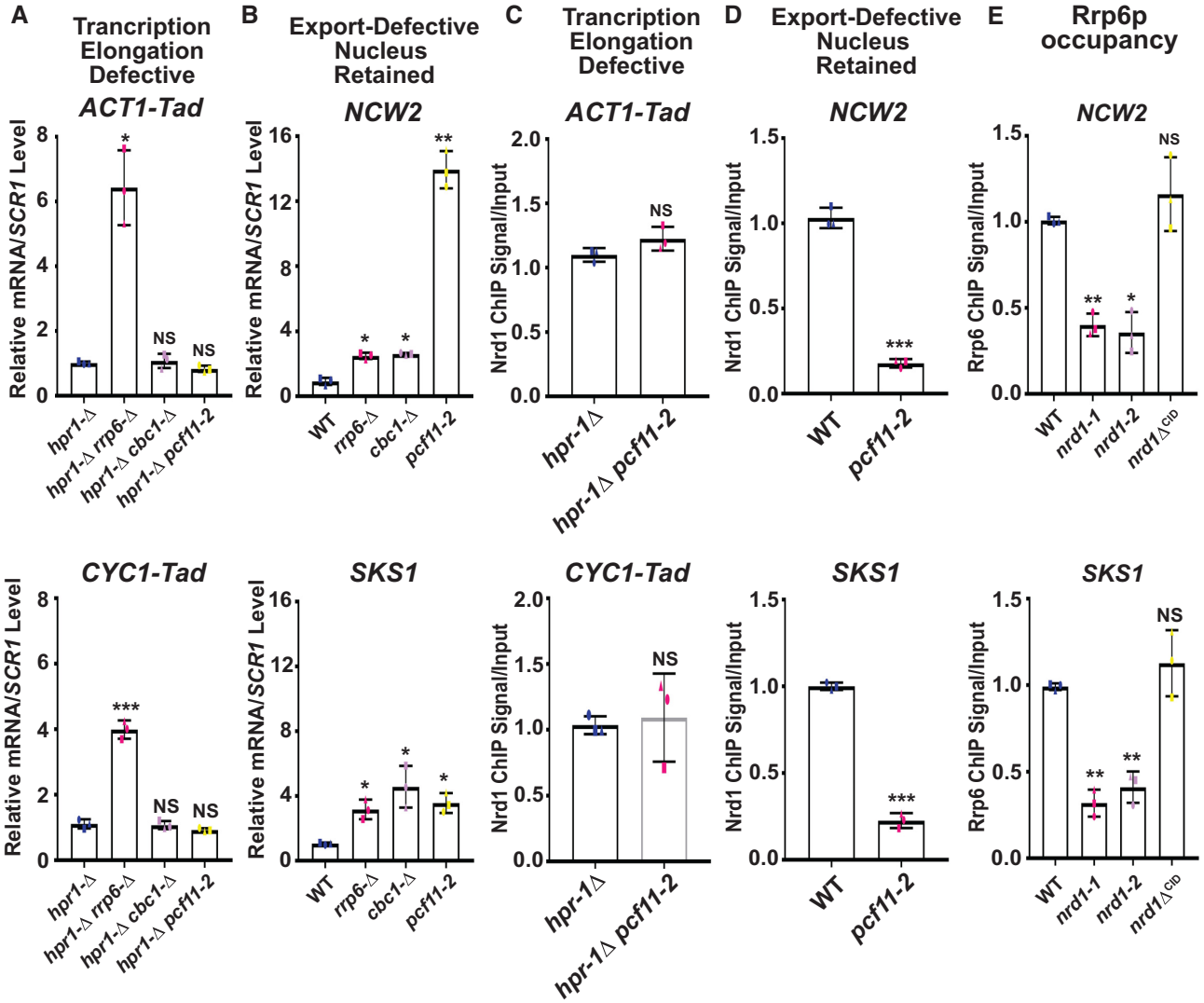

Figure 9. Pcf11p actively contributes to the rapid nuclear decay of export-defective special messages via recruitment of the Nrd1p, which further coordinates the Rrp6p recruitment on to them. (**A** and **B**) Relative steady-state levels of (A) two transcription assembly-defective *ACT1-Tad* and *CYC1-Tad* mRNAs in the indicated isogenic *hpr1*-Δ strain series and (B) two export-inefficient special mRNAs, *NCW2* and *SKS1* in isogenic *pcf11-2* strain series. In both cases, the normalized values of every target mRNA from the wild-type samples was set to 1. As described above, normalized qRT-PCR signals (Mean ± SE) from three independent biological replicates are presented as scatter plots. (**C** and **D**) co-transcriptional recruitment profiles of Nrd1p on (C) transcription assembly-defective *ACT1-Tad* and *CYC1-Tad* messages at 37°C in isogenic *hpr1*-Δ and *hpr1*-Δ *pcf11-2* strains, and (D) two export-incompetent special messages in *NCW2* and *SKS1* at 37°C in an isogenic wild-type and *pcf11-2* strains. (**E**) Occupancy profiles of Rrp6p on the two special mRNAs *NCW2* and S*KS1* at 25°C in the indicated isogenic wild-type (*NRD1*$^{+}$), *nrd1-1*, *nrd1-2* and *nrd1*Δ^{CID} yeast strains. All immunoprecipitations using specific Nrd1p or Rrp6p antibody followed by the recovery of the precipitated DNA and qPCR analyses were performed exactly as described in materials and methods and the legend of Figure 8. *P*-values estimated from Student's two-tailed *t*-tests for a given pair of test strains for each message are presented with the following symbols; **P* < 0.05, ***P* < 0.005 and ****P* < 0.001, NS, not significant.

the export-defective messages thus prompted us to evaluate whether Pcf11p participates in the decay of export-defective mRNAs independently of the CF1A complex. Thus, we determined the steady-state levels of two export-defective, *IMP3,* and *NCW2,* and one typical message, *ACT1,* in wild-type and temperature-sensitive *rna14-1*, *rna15-2* and *clp1-769-5* mutant strains at both 25 and 37°C. The data revealed no stabilization of any export-defective mRNAs in any of these mutant strains at 37°C (Supplementary Figure S4A–C). Consistently, no difference in the decay rates of any of these special mRNAs in wild-type and *rna14-1*, *rna15-2* and *clp1-769-5* mutant strains was observed (Supplementary Figure S4D). To corroborate this finding, we further verified the co-transcriptional recruitment profiles of Nrd1p on one typical (*ACT1*) and two special mRNAs (*IMP3* and *NCW2*) in the yeast strains carrying the mutant alleles of three CF1A components, *rna14-1*, *rna15-2* and *clp1-769-5* (Supplementary Figure S5). The Nrd1p recruitment profiles unveiled no significant difference between the *rna14-1*, *rna15-2*, *clp1-769-5* yeast strains and their corresponding wild-type background. Collectively, these findings strongly argue that Pcf11p participates independently from the CF1A complex in the recruitment of Nrd1p onto the export-defective messages

to promote their exosome/CTEXT-dependent nuclear degradation.

Next, we demonstrated that Rrp6p occupancy profiles on the two special mRNAs, *NCW2* and *SKS1,* is very high in both the *NRD1*$^{+}$ and *nrd1*Δ^{CID} mutant strains, whereas it is significantly low in *nrd1-1* and *nrd1-2* strains (Figure 9E). These data suggest that the Nrd1p recruitment on the aberrant export defective mRNAs leads to the further recruitment of the exosome component Rrp6p on to export-incompetent messages. This finding strongly supports our conclusion that co-transcriptional recruitment of Nrd1p onto the export-defective aberrant messages (mediated by Pcf11p) is followed by the subsequent recruitment of the nuclear exosome, thereby stimulating their rapid nuclear decay. Thus, our collective experimental findings are consistent with the conclusion that in *S. cerevisiae,* the trimeric Nrd1p-Nab3p-Sen1p complex participates universally in the nuclear decay of representative mRNAs from all aberrant categories and that its co-transcriptional recruitment is crucial for the nuclear degradation of every class of aberrant messages.

Several export-incompetent, nucleus-retained mRNAs naturally harbor the Nrd1p RNA-binding motif in their coding regions and have been demonstrated to bind Nrd1p under normal conditions

Previous analysis of the Nrd1p PAR-CLIP data revealed that Nrd1p binds to the UGUAG motif (56,85,86), which is overrepresented in the 3′-end of the non-coding RNA genes and is generally lacking in the mRNAs except those whose expression is regulated by Nrd1p. The susceptibility of the export-defective, special mRNAs to the 'Nrd1p-Sen1p-Nab3p' under normal conditions in wild-type strains prompted us to determine if binding of Nrd1p to any of these mRNAs is a strict requirement of their Nrd1p-dependent degradation. To address this issue systematically, we first evaluated if any of the export incompetent special mRNAs harbor any Nrd1p-binding site(s) and bind Nrd1p *in vivo*. Accordingly, we analyzed the processed wig and FASTA files associated with the published Nrd1p PAR-CLIP dataset GSE31764 Gene Expression Omnibus (http://www.ncbi.nlm.nih.gov/geo/query/acc.cgi?acc=GSE31764) (56). Three of the four experimentally tested special mRNAs, *IMP3* (data not shown)*, NCW2* and *GIC2,* displayed strong Nrd1p cross-linked sites in their coding region (Figure 10C and D). Moreover, the Nrd1p-motif perfectly overlaps with the sites of T→C transition caused by Nrd1p crosslinking to the mRNA by PAR-CLIP, thereby bolstering the notion that Nrd1p binds to the GUAG motif *in vivo* for both of these mRNAs (Figure 10C and D). In contrast, our analysis found no Nrd1p binding sites in the coding regions of two typical mRNAs, *ACT1* and *CYC1* (Figure 10A and B). Notably, we did not expect to find strong mRNA binding motifs in the coding regions of any of the model representative mRNAs, as Nrd1p does not target them under permissive conditions or in wild-type strains. We believe that the nature of co-transcriptional recruitment/binding of Nrd1p onto these messages under the conditional temperature of 37°C is different from its binding to the specific Nrd1 target messages (such as *NRD1*, *PCF11*, *NCW2* and *IMP3* mRNAs; see Discussion section).

To further evaluate whether Nrd1p binds to *NCW2* and *GIC2* mRNAs *in vivo*, we destroyed the tetrameric Nrd1p binding sites of these two RNAs by altering two nucleotides simultaneously in each of *NCW2* and *GIC2* messages and determine if this change leads to the enhancement of their steady-state levels due to diminished decay. To impose a minimal perturbation in the corresponding mutant proteins, we altered the nucleotide residues in *NCW2* and *GIC2* so that only one amino acid underwent substitution from valine to leucine in both cases (Figure 10E and F). Comparison of the steady-state levels of the mutant *ncw2-1* and *gic2-1* mRNAs relative to their wild-type versions revealed a significant (≈4- to 5-fold) enhancement (Figure 10G and I). Furthermore, analysis of their steady-state levels in various *nrd1* mutant yeast strains showed no significant stabilization relative to the *NRD1*$^{+}$ strain. These findings strongly suggest that the physical binding of Nrd1p to its cognate binding sites on the *NCW2* and *GIC2* transcripts is a strict requirement for Nrd1p-dependent degradation of these special mRNAs.

Thus, the experimental evidence presented above collectively supports the conclusion that the Nrd1p-Nab3p-Sen1p complex constitutes a pivotal component of the nuclear surveillance mechanism in *S. cerevisiae* and Nrd1p binding to target aberrant messages is crucial for their nuclear decay. The findings further support the conclusion that, at least for the aberrant export defective messages, the co-transcriptional recruitment of this complex promotes the subsequent recruitment of the nuclear exosome to facilitating their degradation. Thus, the Nrd1p-Nab3p-Sen1p complex appears to serve as an exosome-specificity factor that co-transcriptionally recognizes aberrant mRNAs very early in the transcription and mRNP biogenesis.

DISCUSSION

Despite previous findings supporting a differential distribution of duty among the two exosomal cofactors, TRAMP and CTEXT, and their stage-specific participation in the degradation of aberrant mRNAs (12), the mechanism of stage-specific recognition of distinct aberrant transcripts remained obscure. Further, although the existence of an 'Exosome Specificity Factor' (ESF) was theoretically hypothesized (4,33), its existence and functionality remained elusive. Recently, Nrd1p was demonstrated to facilitate the exosomal degradation of Rho-induced transcription-elongation processing defective (87) mRNPs in *S. cerevisiae* (46,47). Notwithstanding unraveling a key role of Nrd1p in the degradation of these faulty messages, NNS was not demonstrated as the primary recruiter of Rrp6p. Furthermore, its contribution to the degradation of the faulty nuclear mRNAs belonging to every possible aberrant class was not previously addressed.

Physical interaction between Nrd1p and the cap-binding component Cbc1p (a key component of CTEXT) and exosome component Rrp6p (33) inspired us to address the functional role of the NNS complex in the nuclear mRNA decay. This inspiration was further bolstered when the TRAMP4 component Trf4p was reported to inter-

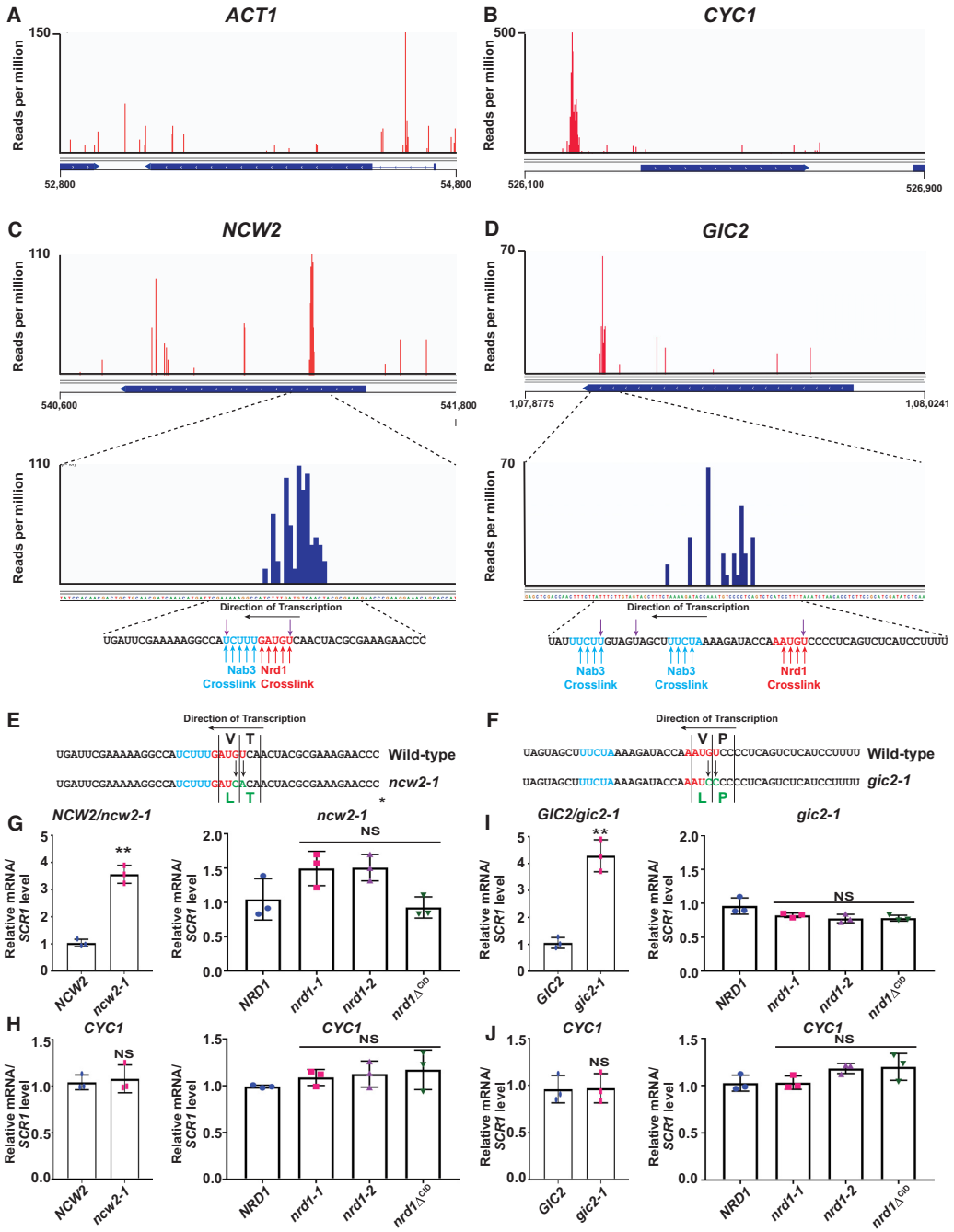

Figure 10. *NCW2* and *GIC2* RNAs harbor functional Nrd1p and Nab3p binding sites. (**A**–**D**) *In vivo* Nrd1p and Nab3p cross-linking sites on *NCW2* and *GIC2* special mRNAs. Cross-linking and binding profiles of Nrd1p from (A) a 2000 nucleotide genomic region of chromosome VI harboring *ACT1*; (B) 800-nucleotide region of chromosome X harboring *CYC1*; (C) 1200-nucleotide region of chromosome XII harboring *NCW2* and (D) 1500 nucleotide region of chromosome IV harboring *GIC2* gene. A higher-resolution map of cross-linked reads to the *NCW2* and *GIC2* coding region is shown at the bottom of the original reads. The number of reads per 10^7 reads is indicated on the y-axis. Sequences of the major cross-linked regions are presented at the bottom of the figure. The upwards arrows correspond to the Nrd1 (blue) or Nab3 (red) cross-linking motifs, and the downward purple arrows indicate the sites most frequently underwent T→C transitions in both Nrd1 and Nab3p data sets. (**E** and **F**) Schematic representations of the sequences of the relevant RNA segments (around the Nrd1p/Nab3p binding sites) of *NCW2* and *ncw2-1* (E), and *GIC2* and *gic2-1* alleles (F). The *ncw2-1* and *gic2-1* alleles were created by site-directed mutagenesis as described in Materials and Methods section. The specific changes made in the nucleotides to destroy the Nrd1p binding site in each RNA are indicated by black arrowheads. Corresponding alterations in the amino acid residues in each case are indicated in green letters below the RNA sequence. The specific codons were also indicated by vertical black lines. (**G** and **J**) Relative steady-state levels of *NCW2* and its variant *ncw2-1* (G), and *GIC2* and its variant *gic2-1* (I) mRNAs, and one export-efficient typical mRNA, *CYC1* (H–J), at 25°C in the indicated wild-type, *nrd1-1*, *nrd1-2* and *nrd1*Δ^{CID} yeast strains. The normalized value of each specific mRNAs from the wild-type sample was set to 1. Three independent samples of random-primed cDNA (biological replicates, $N = 3$) were prepared from the indicated isogenic strains grown at 25°C before subjecting them to real-time qPCR analysis using primer sets specific for each mature mRNA. Transcript copy numbers/3 ng cDNA were normalized to *SCR1* RNA levels in respective samples and are shown as means ± SE. *P*-values estimated from the Student's two-tailed *t*-test for a given pair of test strains for each message are presented with the following symbols, $*P < 0.05$, $**P < 0.005$ and $***P < 0.001$, NS, not significant.

Table 4. Recruitment profiles of Nrd1p on various aberrant nuclear mRNA targets.

	Nrd1p recruitment			
Recruiter	Transcription-assembly-defective	Intron-containing Splice-defective	Transcription-termination defective read-through transcripts with long 3′-Extension	Export-defective
RNAPII	+	+	+	–
Pcf11p	–	–	–	+

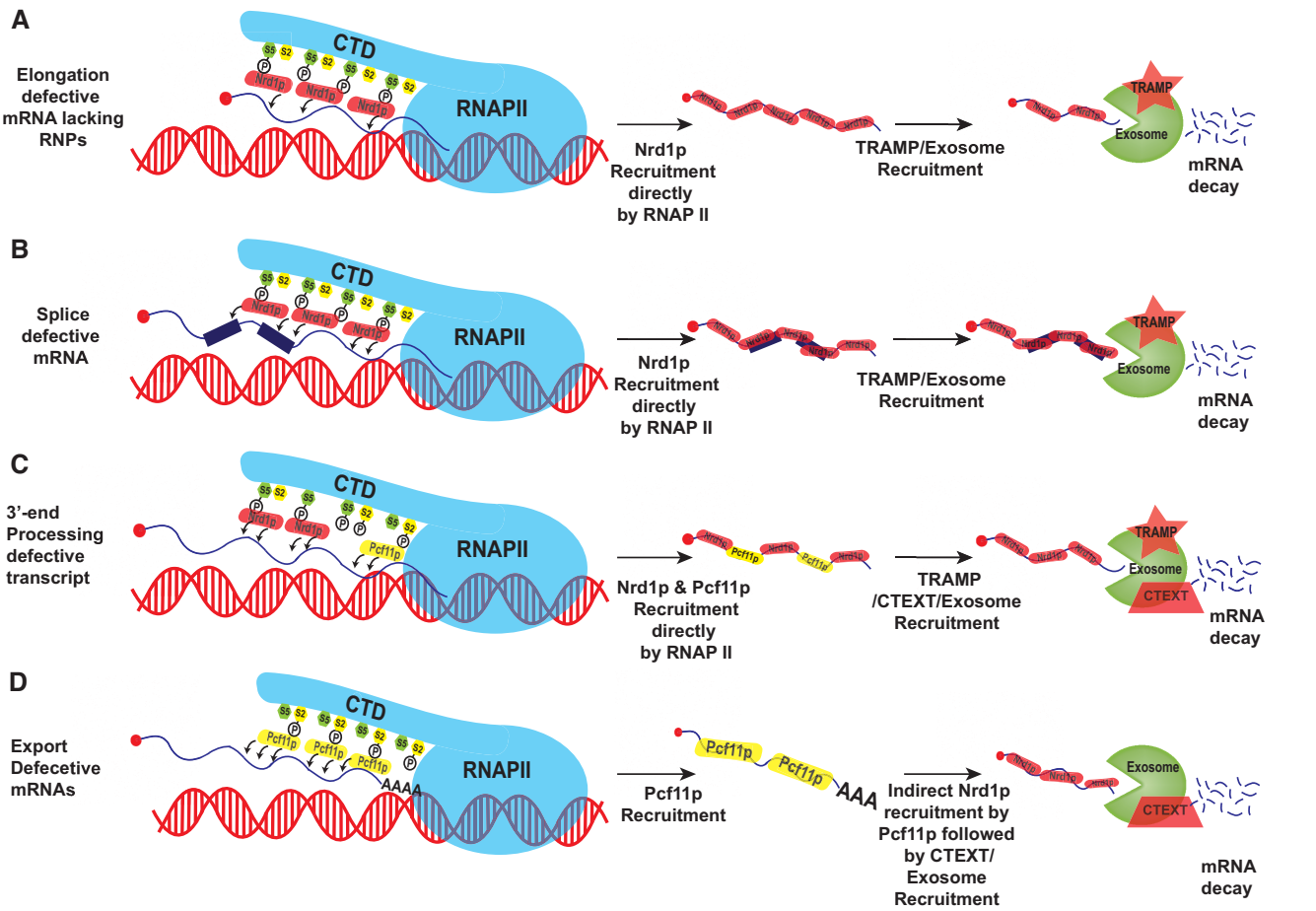

Figure 11. Model elucidating the Nrd1p-dependent recognition and degradation of transcription-assembly-defective (**A**), splice-defective (**B**), 3′-end processing defective (**C**) and export-defective (**D**) messages in Baker's yeast. During transcription initiation, elongation, and termination steps, each message is monitored for the existence of aberrancies, probably by RNAP II. Nrd1p is recruited either directly (A and B) on to the transcription-assembly- and splice-defective messages during the initial stages of transcription/mRNP biogenesis (RNAPII-CTD predominantly consists of Ser-5 marks) leading to the recruitment of the TRAMP/exosome, or indirectly via Pcf11p (D) on to the export-defective messages during the late stage of mRNP biogenesis (RNAPII-CTD predominantly consists of Ser-2 marks) leading to the recruitment of CTEXT/exosome. During the intermediate phase of mRNP biogenesis (RNAPII-CTD primarily carries Ser-5–2 marks), Nrd1p is recruited both directly by RNAPII-CTD as well as indirectly by Pcf11p, leading to the recruitment of TRAMP/CTEXT/exosome. In every case, the recruitment of the exosome on to the aberrant messages leads to their nuclear degradation. In (B), the tiny blue boxes depict the introns.

act with Nrd1p (88). As presented above, our results revealed that Nrd1p (and possibly NNS complex) participates in the degradation of a variety of faulty mRNPs produced at different phases of mRNP maturation and the recruitment of Nrd1p (and possibly NNS) to specific messages is essential for their decay. While RNAPII plays an active role in the co-transcriptional recruitment of Nrd1p during transcription elongation, splicing, and 3′-end processing events via the RNAPII–CTD–Ser5–Nrd1p–CID interaction, its recruitment on to the export inefficient message is mediated by Pcf11p, via RNAPII–CTD–Ser2–Pcf11p–CID interaction (Table 4, Figures 8, 9 and 11A,B). This finding implied that in the terminal phase of mRNP biogenesis, Nrd1p-RNAPII is displaced by Pcf11p-RNAPII once the RNAPII is phosphorylated at Ser2 (Figure 11). Substitution at the RNAPII-CTD is followed by the Nrd1p (NNS complex) recruitment on the aberrant mRNAs by Pcf11p (Figure 11D). Alternatively, Pcf11p may directly recruit Nrd1p post-transcriptionally onto the export-defective messages without any involvement of RNAPII.

It is not clear why Pcf11p is required for the recruitment of Nrd1p onto the export-defective messages. Perhaps these messages may not have a strong association with RNAPII after the cleavage/polyadenylation reaction. They might lose their association with RNAPII at this stage while remaining attached to the transcription foci. This loose association would necessitate the involvement of Pcf11p for their identification as aberrant RNA via the recruitment of Nrd1p. Future work is necessary to unravel this apparent mystery. Notably, Pcf11p was previously demonstrated to participate and co-ordinate mRNA cleavage/polyadenylation as a part of the CF1A complex (80,84). Remarkably, unlike 3′-end maturation, the Pcf11p-dependent co-ordination of Nrd1p recruitment does not require the involvement of other CF1A members (Rna14p, Rna15p and Clp1p) (Supplementary Figures S4 and S5) suggesting a CF1A-independent function.

Nevertheless, our findings hint at the exciting possibility that by acting as an ESF, the NNS complex coordinates the recruitment of either TRAMP or CTEXT differentially onto distinct subsets of faulty messages (Figures 7, 8 and 10). Although the underlying mechanism is still elusive, Nrd1p recruitment via RNAPII–Ser5–CTD–Nrd1p–CID interaction appears critical for the selective recruitment of TRAMP to target transcription elongation splice-defective messages. In contrast, its recruitment via RNAPII–Ser2–CTD–Pcf11p–CID interaction seems vital for further recruiting CTEXT to target export defective messages for decay (Figure 11). Indeed, this conclusion explains our finding that the nuclear decay of the aberrantly long 3′-extended read-through transcripts requires the combined activity of TRAMP and CTEXT. Notably, these 3′-extended transcripts are produced during the intermediate mRNP biogenesis phase when the predominant population of RNAPII-CTD remains hyperphosphorylated, consisting of both Ser5/Ser2 marks (89–91). Since both Nrd1p and Pcf11p may remain associated with the hyperphosphorylated RNAPII-CTD having both Ser5-P/Ser2-P marks (78,92–94), this situation subsequently recruits both TRAMP (by Nrd1p) and CTEXT (by Pcf11p) onto these read-through transcripts presumably in the long 3′-extended segments (Figure 11C). Our observation is consistent with the finding that recruitment of Nrd1p onto these read-through messages in *nrd1*Δ^{CID} strain was not as low (approximately 40–50% compared to *NRD1*$^{+}$ strain, Figure 8F) as those found in the cases of transcription elongation-defective and splice-defective messages (approximately 5–20% compared to *NRD1*$^{+}$ strain, Figure 8D and E). These data strongly imply that in the *nrd1*Δ^{CID} yeast strain, the remaining 40–50% of the Nrd1p recruited on to these 3′-extended faulty messages was carried out via Pcf11p dependent manner.

Mining and re-analysis of genome-wide Nrd1p and Nab3p binding maps obtained from PAR-CLIP (22,56,85) revealed that the yeast mRNAome generally lacks the Nrd1p and Nab3p sites, except several mRNAs, such as *NRD1*, *URA2*, *URA8*, *PCF11*, *FKS2* that are enriched with these sites (16,18, 47–49). Susceptibility of the export-defective, special messages, *SKS1*, *IMP3*, *NCW2* and *GIC2* to the Nrd1p-Nab3p-Sen1p complex under normal conditions in wild-type cells prompted us to test if any of these mRNAs display any Nrd1p/Nab3p binding *in vivo*. As shown in Figure 10, analysis of the PAR-CLIP data revealed that *NCW2* and *GIC2* messages harbor Nrd1p/Nab3p motifs and display Nrd1p/Nab3p binding *in vivo* demonstrated by an overlapping T→C transitions (Figure 10C and D). Mutating specific nucleotide residues within these potential Nrd1p-binding sites in *NCW2* and *GIC2* mRNAs led to their significant stabilization in the *NRD1*$^{+}$ strain. Furthermore, the steady-state levels displayed by these mutant messages in all the *nrd1* mutant strains did not show any further enhancement (Figure 10G–I), thereby suggesting that Nrd1p binding to these special messages is a strict requirement for their decay. Destroying the Nrd1p binding site (*cis*-element) on these messages by site-specific alteration of the nucleotides or inactivating/depleting the Nrd1p (*trans*-acting factor) resulted in the abolition of their nuclear decay. Thus, the evidence presented in Figure 9A–E strongly supports the idea that Nrd1p/Nab3p binds to these mRNA targets and recruits the exosome/Rrp6p to facilitate their degradation. Interestingly, a thorough search for the putative Nrd1p/Nab3p binding motifs in the model transcription-elongation-defective (*ACT1-Tad* and *CYC1-Tad*), splice-defective (pre-*ACT1* and pre-*CYH2*), and 3′-end processing defective (*LYS2-Ex* and *CYC1-Ex*) mRNAs did not yield any well-defined motif (Figure 10A and B). However, the co-transcriptional recruitment profiles of some of these mRNAs strongly suggest that, indeed, Nrd1p preferentially binds to them when they are derived as aberrant/faulty messages. Thus, we favor the view that the nature of the Nrd1p/Nab3p binding to the global or specific aberrant mRNAs is fundamentally different from their binding to the sites harboring the defined motif such as snoRNAs, snRNAs, CUTs and the Nrd1p-target messages (*NRD1*, *URA2*, *URA8*, etc.). This view is supported by the finding that triggering the transcriptome-wide expression of aberrant mRNAs via induction of Rho protein led to the redistribution of the majority of the cellular Nrd1/Nab3p to the loci of protein-coding genes from snRNA/snoRNA loci (47). Notably, most of these protein-coding mRNAs do not harbor any defined Nrd1p/Nab3p motif. Future research directed to determine the binding sites on these aberrant messages produced under the conditional temperature of 37°C would resolve this issue.

Our data imply that the NNS complex qualifies well as a universal ESF by virtue of (i) exhibiting a uniform affinity to all categories of aberrant nuclear messages and (ii) having an ability to identify and delineate a distinct set of aberrant messages from a massive pool of cellular mRNAs via its increased occupancy on these messages. This conclusion is strongly supported by the increased co-transcriptional recruitment observed onto the aberrant mRNA targets generated in THO mutant strains (e.g., mRNAs from *hpr1*-Δ at 37°C compared to 25°C, see Figure 8A and B) or onto the special messages (*NCW2* versus *CYC1*, see Figure 8C). Even though the molecular basis of the distinction between the normal/functional and aberrant/faulty messages is not clear at this point, it appears from this work that this difference may be accomplished co-transcriptionally by the presence of Nrd1p, which is selectively recruited to the aberrant messages (Figure 8A–C). It is reasonable to assume that during transcription elongation, a competi-

tion exists between the binding of the mRNP biogenesis factors (such as THO/splicing/export factors) and the association of NNS with the transcribing messages. In the case of a normal message, the mRNP biogenesis factors are promptly deposited on the maturing message, excluding the binding of the Nrd1p. During the transcription elongation of the aberrant messages, in contrast, binding of processing factors becomes impaired, leading to retardation of the speed of transcription, allowing more time for NNS to bind co-transcriptionally to these aberrant messages. However, it is currently unknown whether RNAPII actively coordinates the selective recruitment of Nrd1p onto specific types of aberrant messages during various phases of transcription elongation and mRNP maturation events. Alternatively, targeted Nrd1p recruitment on to aberrant messages may also result from the competition between the mRNP biogenesis and NNS complex, as described above. Nevertheless, this mystery provides us with an opportunity to investigate further the distinguishing feature(s) of aberrant messages that lead to the subsequent recruitment of Nrd1p (possibly NNS complex) to facilitate their degradation.

DATA AVAILABILITY

All the raw data leading to establishing the final results presented here are available in the supplementary material as a separate excel file '**SinghP21 NAR Res Art Revised Raw Data**'.

SUPPLEMENTARY DATA

Supplementary Data are available at NAR Online.

ACKNOWLEDGEMENTS

We gratefully acknowledge Dr. Stephen Buratowski (Department of Biological Chemistry and Molecular Pharmacology, Harvard Medical School, Boston, MA, U.S.A.) for kindly sharing *nrd1-1*, *nrd1-2*, *nrd1*Δ^{CID}, *sen1-1* mutant strains, anti-Nrd1 antibody and various *NRD1* plasmids. We also acknowledge Dr Maurice Swanson (University of Florida, Gainesville, FL, U.S.A.), Dr. Jeffry Corden (Johns Hopkins School of Medicine, Baltimore, MD, U.S.A.) for *nab3-10* strain, Dr Athar Ansari (Wayne State University, Michigan, U.S.A.) for the *pcf11-2, and clp1-769-5* mutant yeast strains, and Dr. Scott Butler for providing us with the Anti-Rrp6p, Anti-Rrp4p, Anti-Cbc1p, and Anti-Tif4631 antibodies (University of Rochester, Rochester, NY, U.S.A.). We thank Dr Scott Butler, Dr Satarupa Das, Dr Arindam Chakraborty, and the members of the Das Laboratory for critically reading this manuscript. We also thank the anonymous reviewers for their critical comments and constructive suggestions.

FUNDING

DBT [BT/PR27917/BRB/10/ 1673/2018 to B.D., M.B.]; Jadavpur University [RUSA 2.0 Research Grant to B.D.]; Government of West Bengal (to P.S.); CSIR [38(1427)/16/EMR-II to A.C.]. [BT/PR27917/BRB/10/ 1673/2018].

Conflict of interest statement. None declared.

REFERENCES

1. Parker,R. (2012) RNA degradation in Saccharomyces cerevisae. *Genetics*, **191**, 671–702.
2. Das,S. and Das,B. (2013) mRNA quality control pathways in Saccharomyces cerevisiae. *J. Biosci.*, **38**, 615–640.
3. Mitchell,P. (2014) Exosome substrate targeting: the long and short of it. *Biochem. Soc. Trans.*, **42**, 1129–1134.
4. Kilchert,C., Wittmann,S. and Vasiljeva,L. (2016) The regulation and functions of the nuclear RNA exosome complex. *Nat. Rev. Mol. Cell Biol.*, **17**, 227–239.
5. Mitchell,P., Petfalski,E., Shevchenko,A., Mann,M. and Tollervey,D. (1997) The exosome: a conserved eukaryoticRNA processing complex containing multiple 3′→5′ exoribonucleases. *Cell*, **91**, 457–466.
6. Butler,J.S. (2002) The yin and yang of the exosome. *Trends Cell Biol.*, **12**, 90–96.
7. Allmang,C., Mitchell,P., Petfalski,E. and Tollervey,D. (2000) Degradation of ribosomal RNA precursors by the exosome. *Nucleic Acids Res.*, **28**, 1684–1691.
8. Briggs,M.W., Burkard,K.T. and Butler,J.S. (1998) Rrp6p, the yeast homologue of the human PM-Scl 100-kDa autoantigen, is essential for efficient 5.8 S rRNA 3′ end formation. *J. Biol. Chem.*, **273**, 13255–13263.
9. Schmidt,K. and Butler,J.S. (2013) Nuclear RNA surveillance: role of TRAMP in controlling exosome specificity. *Wiley Interdiscip Rev RNA*, **4**, 217–231.
10. Halbach,F., Reichelt,P., Rode,M. and Conti,E. (2013) The yeast ski complex: crystal structure and RNA channeling to the exosome complex. *Cell*, **154**, 814–826.
11. Hardwick,S.W. and Luisi,B.F. (2013) Rarely at rest: RNA helicases and their busy contributions to RNA degradation, regulation and quality control. *RNA Biol*, **10**, 56–70.
12. Maity,A., Chaudhuri,A. and Das,B. (2016) DRN and TRAMP degrade specific and overlapping aberrant mRNAs formed at various stages of mRNP biogenesis in Saccharomyces cerevisiae. *FEMS Yeast Res.*, **16**, fow088.
13. Das,B., Guo,Z., Russo,P., Chartrand,P. and Sherman,F. (2000) The role of nuclear cap binding protein Cbc1p of yeast in mRNA termination and degradation. *Mol. Cell. Biol.*, **20**, 2827–2838.
14. Das,B., Butler,J.S. and Sherman,F. (2003) Degradation of normal mRNA in the nucleus of Saccharomyces cerevisiae. *Mol. Cell. Biol.*, **23**, 5502–5515.
15. Das,B., Das,S. and Sherman,F. (2006) Mutant LYS2 mRNAs retained and degraded in the nucleus of Saccharomyces cerevisiae. *Proc. Natl. Acad. Sci. U.S.A.*, **103**, 10871–10876.
16. Das,S., Saha,U. and Das,B. (2014) Cbc2p, Upf3p and eIF4G are components of the DRN (Degradation of mRNA in the Nucleus) in Saccharomyces cerevisiae. *FEMS Yeast Res.*, **14**, 922–932.
17. Arigo,J.T., Carroll,K.L., Ames,J.M. and Corden,J.L. (2006) Regulation of yeast NRD1 expression by premature transcription termination. *Mol. Cell*, **21**, 641–651.
18. Conrad,N.K., Wilson,S.M., Steinmetz,E.J., Patturajan,M., Brow,D.A., Swanson,M.S. and Corden,J.L. (2000) A yeast heterogeneous nuclear ribonucleoprotein complex associated with RNA polymerase II. *Genetics*, **154**, 557–571.
19. Steinmetz,E.J., Conrad,N.K., Brow,D.A. and Corden,J.L. (2001) RNA-binding protein Nrd1 directs poly(A)-independent 3′-end formation of RNA polymerase II transcripts. *Nature*, **413**, 327–331.
20. Steinmetz,E.J. and Brow,D.A. (1998) Control of pre-mRNA accumulation by the essential yeast protein Nrd1 requires high-affinity transcript binding and a domain implicated in RNA polymerase II association. *Proc. Natl. Acad. Sci. U. S. A.*, **95**, 6699–6704.
21. Mayer,A., Heidemann,M., Lidschreiber,M., Schreieck,A., Sun,M., Hintermair,C., Kremmer,E., Eick,D. and Cramer,P. (2012) CTD Tyrosine phosphorylation impairs termination factor recruitment to RNA polymerase II. *Science*, **336**, 1723–1725.
22. Schulz,D., Schwalb,B., Kiesel,A., Baejen,C., Torkler,P., Gagneur,J., Soeding,J. and Cramer,P. (2013) Transcriptome surveillance by selective termination of noncoding RNA synthesis. *Cell*, **155**, 1075–1087.

23. Cloutier,S.C., Ma,W.K., Nguyen,L.T. and Tran,E.J. (2012) The DEAD-box RNA helicase Dbp2 connects RNA quality control with repression of aberrant transcription. *J. Biol. Chem.*, **287**, 26155–26166.
24. Kuai,L., Das,B. and Sherman,F. (2005) A nuclear degradation pathway controls the abundance of normal mRNAs in Saccharomyces cerevisiae. *Proc. Natl. Acad. Sci. U.S.A.*, **102**, 13962–13967.
25. Sarkar,D., Paira,S. and Das,B. (2018) Nuclear mRNA degradation tunes the gain of the unfolded protein response in Saccharomyces cerevisiae. *NucleicAcidsRes.*, **46**, 1139–1156.
26. Das,S., Biswas,S., Chaudhuri,S., Bhattacharyya,A. and Das,B. (2019) A nuclear zip code in SKS1 mRNA promotes its slow export, nuclear retention, and degradation by the nuclear exosome/DRN in saccharomyces cerevisiae. *J. Mol. Biol.*, **431**, 3626–3646.
27. Porrua,O. and Libri,D. (2013) A bacterial-like mechanism for transcription termination by the Sen1p helicase in budding yeast. *Nat. Struct. Mol. Biol.*, **20**, 884–891.
28. Tuck,A.C. and Tollervey,D. (2013) A transcriptome-wide atlas of RNP composition reveals diverse classes of mRNAs and lncRNAs. *Cell*, **154**, 996–1009.
29. Steinmetz,E.J. and Brow,D.A. (1996) Repression of gene expression by an exogenous sequence element acting in concert with a heterogeneous nuclear ribonucleoprotein-like protein, Nrd1, and the putative helicase Sen1. *Mol. Cell. Biol.*, **16**, 6993–7003.
30. Steinmetz,E.J., Conrad,N.K., Brow,D.A. and Corden,J.L. (2001) RNA-binding protein Nrd1 directs poly(A)-independent 3′-end formation of RNA polymerase II transcripts. *Nature*, **413**, 327–331.
31. Seidah,N.G., Poirier,S., Denis,M., Parker,R., Miao,B., Mapelli,C., Prat,A., Wassef,H., Davignon,J., Hajjar,K.A. *et al.* (2012) Annexin A2 is a natural extrahepatic inhibitor of the PCSK9-induced LDL receptor degradation. *PLoS One*, **7**, e41865.
32. Arigo,J.T., Eyler,D.E., Carroll,K.L. and Corden,J.L. (2006) Termination of cryptic unstable transcripts is directed by yeast RNA-binding proteins Nrd1 and Nab3. *Mol. Cell*, **23**, 841–851.
33. Vasiljeva,L. and Buratowski,S. (2006) Nrd1 interacts with the nuclear exosome for 3′ processing of RNA polymerase II transcripts. *Mol. Cell*, **21**, 239–248.
34. Corden,J.L. (2013) RNA polymerase II C-terminal domain: Tethering transcription to transcript and template. *Chem. Rev.*, **113**, 8423–8455.
35. Eick,D. and Geyer,M. (2013) The RNA polymerase II carboxy-terminal domain (CTD) code. *Chem. Rev.*, **113**, 8456–8490.
36. Harlen,K.M. and Churchman,L.S. (2017) The code and beyond: Transcription regulation by the RNA polymerase II carboxy-terminal domain. *Nat. Rev. Mol. Cell Biol.*, **18**, 263–273.
37. Jeronimo,C., Collin,P. and Robert,F. (2016) The RNA Polymerase II CTD: The increasing complexity of a low-complexity protein domain. *J. Mol. Biol.*, **428**, 2607–2622.
38. Milligan,L., Huynh-Thu,V.A., Delan-Forino,C., Tuck,A., Petfalski,E., Lombraña,R., Sanguinetti,G., Kudla,G. and Tollervey,D. (2016) Strand-specific, high-resolution mapping of modified RNA polymerase II. *Mol. Syst. Biol.*, **12**, 874.
39. Collin,P., Jeronimo,C., Poitras,C. and Robert,F. (2019) RNA polymerase II CTD tyrosine 1 is required for efficient termination by the Nrd1-Nab3-Sen1 pathway. *Mol. Cell*, **73**, 655–669.
40. Larochelle,M., Robert,M.A., Hébert,J.N., Liu,X., Matteau,D., Rodrigue,S., Tian,B., Jacques,P.É. and Bachand,F. (2018) Common mechanism of transcription termination at coding and noncoding RNA genes in fission yeast. *Nat. Commun.*, **9**, 4364–4378.
41. Han,Z., Libri,D. and Porrua,O. (2017) Biochemical characterization of the helicase Sen1 provides new insights into the mechanisms of non-coding transcription termination. *Nucleic Acids Res.*, **45**, 1355–1370.
42. Hazelbaker,D.Z., Marquardt,S., Wlotzka,W. and Buratowski,S. (2013) Kinetic competition between RNA Polymerase II and Sen1-dependent transcription termination. *Mol. Cell*, **49**, 55–66.
43. Bresson,S., Tuck,A., Staneva,D. and Tollervey,D. (2017) Nuclear RNA decay pathways aid rapid remodeling of gene expression in yeast. *Mol. Cell*, **65**, 787–800.
44. Creamer,T.J., Darby,M.M., Jamonnak,N., Schaughency,P., Hao,H., Wheelan,S.J. and Corden,J.L. (2011) Transcriptome-wide binding sites for components of the Saccharomyces cerevisiae non-poly(A) termination pathway: Nrd1, Nab3, and Sen1. *PLos Genet.*, **7**, e1002329.
45. Jamonnak,N., Creamer,T.J., Darby,M.M., Schaughency,P., Wheelan,S.J. and Corden,J.L. (2011) Yeast Nrd1, Nab3, and Sen1 transcriptome-wide binding maps suggest multiple roles in post-transcriptional RNA processing. *RNA*, **17**, 2011–2025.
46. Honorine,R., Mosrin-Huaman,C., Hervouet-Coste,N., Libri,D. and Rahmouni,A.R. (2011) Nuclear mRNA quality control in yeast is mediated by Nrd1 co-transcriptional recruitment, as revealed by the targeting of Rho-induced aberrant transcripts. *Nucleic Acids Res.*, **39**, 2809–2820.
47. Moreau,K., Le Dantec,A., Mosrin-Huaman,C., Bigot,Y., Piégu,B. and Rahmouni,A.R. (2019) Perturbation of mRNP biogenesis reveals a dynamic landscape of the Rrp6-dependent surveillance machinery trafficking along the yeast genome. *RNA Biol.*, **16**, 879–889.
48. Kuehner,J.N. and Brow,D.A. (2008) Regulation of a Eukaryotic Gene by GTP-Dependent start site selection and transcription attenuation. *Mol. Cell*, **31**, 201–211.
49. Thiebaut,M., Colin,J., Neil,H., Jacquier,A., Séraphin,B., Lacroute,F. and Libri,D. (2008) Futile cycle of transcription initiation and termination modulates the response to nucleotide shortage in S. cerevisiae. *Mol. Cell*, **31**, 671–682.
50. Kim,K.Y. and Levin,D.E. (2011) Mpk1 MAPK association with the paf1 complex blocks sen1-mediated premature transcription termination. *Cell*, **144**, 745–756.
51. Van Nues,R., Schweikert,G., De Leau,E., Selega,A., Langford,A., Franklin,R., Iosub,I., Wadsworth,P., Sanguinetti,G. and Granneman,S. (2017) Kinetic CRAC uncovers a role for Nab3 in determining gene expression profiles during stress. *Nat. Commun.*, **8**, https://doi.org/10.1038/s41467-017-00025-5.
52. Webb,S., Hector,R.D., Kudla,G. and Granneman,S. (2014) PAR-CLIP data indicate that Nrd1-Nab3-dependent transcription termination regulates expression of hundreds of protein coding genes in yeast. *Genome Biol.*, **15**, 15:R8.
53. Sherman,F. (1991) Getting started with yeast. *Methods Enzymol.*, **194**, 3–21.
54. Keogh,M.C. and Buratowski,S. (2004) Using chromatin immunoprecipitation to map cotranscriptional mRNA processing in Saccharomyces cerevisiae. *Methods Mol. Biol.*, **257**, 1–16.
55. Edgar,R., Domrachev,M. and Lash,A.E. (2002) Gene Expression Omnibus: NCBI gene expression and hybridization array data repository. *Nucleic Acids Res.*, **30**, 207–210.
56. Creamer,T.J., Darby,M.M., Jamonnak,N., Schaughency,P., Hao,H., Wheelan,S.J. and Corden,J.L. (2011) Transcriptome-wide binding sites for components of the Saccharomyces cerevisiae non-poly(A) termination pathway: Nrd1, Nab3, and Sen1. *PLos Genet.*, **7**, e1002329.
57. Robinson,J.T., Thorvaldsdóttir,H., Winckler,W., Guttman,M., Lander,E.S., Getz,G. and Mesirov,J.P. (2011) Integrative genomics viewer. *Nat. Biotechnol.*, **29**, 24–26.
58. Leinonen,R., Sugawara,H., Shumway,M. and Collaboration,I.N.S.D. (2011) The sequence read archive. *Nucleic Acids Res.*, **39**, D19–D21.
59. Dobin,A., Davis,C.A., Schlesinger,F., Drenkow,J., Zaleski,C., Jha,S., Batut,P., Chaisson,M. and Gingeras,T.R. (2013) STAR: ultrafast universal RNA-seq aligner. *Bioinformatics*, **29**, 15–21.
60. Afgan,E., Baker,D., Batut,B., van den Beek,M., Bouvier,D., Čech,M., Chilton,J., Clements,D., Coraor,N., Grüning,B.A. *et al.* (2018) The Galaxy platform for accessible, reproducible and collaborative biomedical analyses: 2018 update. *Nucleic Acids Res.*, **46**, W537–W544.
61. Libri,D., Dower,K., Boulay,J., Thomsen,R., Rosbash,M. and Jensen,T.H. (2002) Interactions between mRNA export commitment, 3′-end quality control, and nuclear degradation. *Mol. Cell. Biol.*, **22**, 8254–8266.
62. Strasser,K., Masuda,S., Mason,P., Pfannstiel,J., Oppizzi,M., Rodriguez-Navarro,S., Rondon,A.G., Aguilera,A., Struhl,K., Reed,R. *et al.* (2002) TREX is a conserved complex coupling transcription with messenger RNA export. *Nature*, **417**, 304–308.
63. Zenklusen,D., Vinciguerra,P., Wyss,J.C. and Stutz,F. (2002) Stable mRNP formation and export require cotranscriptional recruitment of the mRNA export factors Yra1p and Sub2p by Hpr1p. *Mol. Cell. Biol.*, **22**, 8241–8253.

64. Rougemaille,M., Gudipati,R.K., Olesen,J.R., Thomsen,R., Seraphin,B., Libri,D. and Jensen,T.H. (2007) Dissecting mechanisms of nuclear mRNA surveillance in THO/sub2 complex mutants. *EMBO J.*, **26**, 2317–2326.
65. Plumpton,M., McGarvey,M. and Beggs,J.D. (1994) A dominant negative mutation in the conserved RNA helicase motif 'SAT' causes splicing factor PRP2 to stall in spliceosomes. *EMBO J.*, **13**, 879–887.
66. Bousquet-Antonelli,C., Presutti,C. and Tollervey,D. (2000) Identification of a regulated pathway for nuclear pre-mRNA turnover. *Cell*, **102**, 765–775.
67. Kong,K.Y.E., Tang,H.M.V., Pan,K., Huang,Z., Lee,T.H.J., Hinnebusch,A.G., Jin,D.Y. and Wong,C.M. (2014) Cotranscriptional recruitment of yeast TRAMP complex to intronic sequences promotes optimal pre-mRNA splicing. *Nucleic Acids Res.*, **42**, 643–660.
68. Birse,C.E., Minvielle-Sebastia,L., Lee,B.A., Keller,W. and Proudfoot,N.J. (1998) Coupling termination of transcription to messenger RNA maturation in yeast. *Science*, **280**, 298–301.
69. Minvielle-Sebastia,L. and Keller,W. (1999) mRNA polyadenylation and its coupling to other RNA processing reactions and to transcription. *Curr. Opin. Cell Biol.*, **11**, 352–357.
70. Proudfoot,N. (2000) Connecting transcription to messenger RNA processing. *Trends Biochem. Sci.*, **25**, 290–293.
71. Yonaha,M. and Proudfoot,N.J. (2000) Transcriptional termination and coupled polyadenylation in vitro. *EMBO J.*, **19**, 3770–3777.
72. Torchet,C., Bousquet-Antonelli,C., Milligan,L., Thompson,E., Kufel,J. and Tollervey,D. (2002) Processing of 3′-extended read-through transcripts by the exosome can generate functional mRNAs. *Mol. Cell*, **9**, 1285–1296.
73. Wente,S.R. and Blobel,G. (1993) A temperature-sensitive NUP116 null mutant forms a nuclear envelope seal over the yeast nuclear pore complex thereby blocking nucleocytoplasmic traffic. *J. Cell Biol.*, **123**, 275–284.
74. Xu,Z., Wei,W., Gagneur,J., Perocchi,F., Clauder-Munster,S., Camblong,J., Guffanti,E., Stutz,F., Huber,W. and Steinmetz,L.M. (2009) Bidirectional promoters generate pervasive transcription in yeast. *Nature*, **457**, 1033–1037.
75. Danielle,B. and Didier,A. (2012) Analysis of co-transcriptional RNA processing by RNA-ChIP assay. *Methods Mol. Biol.*, **809**, 563–577.
76. Obrdlik,A. and Percipalle,P. (2009) Analysis of nascent RNA transcripts by chromatin RNA immunoprecipitation. *Methods Mol. Biol.*, **567**, 215–235.
77. Amrani,N., Minet,M., Wyers,F., Dufour,M.E., Aggerbeck,L.P. and Lacroute,F. (1997) PCF11 encodes a third protein component of yeast cleavage and polyadenylation factor I. *Mol. Cell. Biol.*, **17**, 1102–1109.
78. Barilla,D., Lee,B.A. and Proudfoot,N.J. (2001) Cleavage/polyadenylation factor IA associates with the carboxyl-terminal domain of RNA polymerase II in Saccharomyces cerevisiae. *Proc. Natl. Acad. Sci.*, **98**, 445–450.
79. Licatalosi,D.D., Geiger,G., Minet,M., Schroeder,S., Cilli,K., McNeil,J.B. and Bentley,D.L. (2002) Functional interaction of yeast pre-mRNA 3′ end processing factors with RNA polymerase II. *Mol. Cell*, **9**, 1101–1111.
80. Sadowski,M., Dichtl,B., Hübner,W. and Keller,W. (2003) Independent functions of yeast Pcf11p in pre-mRNA 3′ end processing and in transcription termination. *EMBO J.*, **22**, 2167–2177.
81. Zhang,Z., Fu,J. and Gilmour,D.S. (2005) CTD-dependent dismantling of the RNA polymerase II elongation complex by the pre-mRNA 3′-end processing factor, Pcf11. *Genes Dev.*, **19**, 1572–1580.
82. Singh,N., Ma,Z., Gemmill,T., Wu,X., DeFiglio,H., Rossettini,A., Rabeler,C., Beane,O., Morse,R.H., Palumbo,M.J. *et al.* (2009) The Ess1 prolyl isomerase is required for transcription termination of small noncoding RNAs via the Nrd1 spathway. *Mol. Cell*, **36**, 255–266.
83. Gordon,J.M.B., Shikov,S., Kuehner,J.N., Liriano,M., Lee,E., Stafford,W., Poulsen,M.B., Harrison,C., Moore,C. and Bohm,A. (2011) Reconstitution of CF IA from Overexpressed subunits reveals stoichiometry and provides insights into molecular topology. *Biochemistry*, **50**, 10203–10214.
84. Gross,S. and Moore,C. (2001) Five subunits are required for reconstitution of the cleavage and polyadenylation activities of Saccharomyces cerevisiae cleavage factor I. *Proc. Natl. Acad. Sci. U.S.A.*, **98**, 6080–6085.
85. Jamonnak,N., Creamer,T.J., Darby,M.M., Schaughency,P., Wheelan,S.J. and Corden,J.L. (2011) Yeast Nrd1, Nab3, and Sen1 transcriptome-wide binding maps suggest multiple roles in post-transcriptional RNA processing. *RNA*, **17**, 2011–2025.
86. Wlotzka,W., Kudla,G., Granneman,S. and Tollervey,D. (2011) The nuclear RNA polymerase II surveillance system targets polymerase III transcripts. *EMBO J.*, **30**, 1790–1803.
87. Mosrin-Huaman,C., Honorine,R. and Rahmouni,A.R. (2009) Expression of bacterial rho factor in yeast identifies new factors involved in the functional interplay between transcription and mRNP biogenesis. *Mol. Cell. Biol.*, **29**, 4033–4044.
88. Tudek,A., Porrua,O., Kabzinski,T., Lidschreiber,M., Kubicek,K., Fortova,A., Lacroute,F., Vanacova,S., Cramer,P., Stefl,R. *et al.* (2014) Molecular basis for coordinating transcription termination with noncoding RNA degradation. *Mol. Cell*, **55**, 467–481.
89. Kim,H., Erickson,B., Luo,W., Seward,D., Graber,J.H., Pollock,D.D., Megee,P.C. and Bentley,D.L. (2010) Gene-specific RNA polymerase II phosphorylation and the CTD code. *Nat. Struct. Mol. Biol.*, **17**, 1279–1286.
90. Tietjen,J.R., Zhang,D.W., Rodríguez-Molina,J.B., White,B.E., Akhtar,M.S., Heidemann,M., Li,X., Chapman,R.D., Shokat,K., Keles,S. *et al.* (2010) Chemical-genomic dissection of the CTD code. *Nat. Struct. Mol. Biol.*, **17**, 1154–1161.
91. Mayer,A., Lidschreiber,M., Siebert,M., Leike,K., Söding,J. and Cramer,P. (2010) Uniform transitions of the general RNA polymerase II transcription complex. *Nat. Struct. Mol. Biol.*, **17**, 1272–1278.
92. Vasiljeva,L., Kim,M., Mutschler,H., Buratowski,S. and Meinhart,A. (2008) The Nrd1-Nab3-Sen1 termination complex interacts with the Ser5-phosphorylated RNA polymerase II C-terminal domain. *Nat. Struct. Mol. Biol.*, **15**, 795–804.
93. Kubicek,K., Cerna,H., Holub,P., Pasulka,J., Hrossova,D., Loehr,F., Hofr,C., Vanacova,S. and Stefl,R. (2012) Serine phosphorylation and proline isomerization in RNAP II CTD control recruitment of Nrdl. *Genes Dev.*, **26**, 1891–1896.
94. Lunde,B.M., Reichow,S.L., Kim,M., Suh,H., Leeper,T.C., Yang,F., Mutschler,H., Buratowski,S., Meinhart,A. and Varani,G. (2010) Cooperative interaction of transcription termination factors with the RNA polymerase II C-terminal domain. *Nat. Struct. Mol. Biol.*, **17**, 1195–1201.